RSC Advances

REVIEW

View Article Online
View Journal | View Issue

Cite this: *RSC Adv.*, 2023, **13**, 5833

Recent progress of theoretical studies on electro- and photo-chemical conversion of CO_2 with single-atom catalysts

Liyun Jiang,[a] Qingqing Yang,[a] Zhaoming Xia,[b] Xiaohu Yu,[a] Mengdie Zhao,[a] Qiping Shi[a] and Qi Yu*[ac]

Received 16th December 2022
Accepted 9th February 2023

DOI: 10.1039/d2ra08021d

rsc.li/rsc-advances

The CO_2 reduction reaction (CO_2RR) into chemical products is a promising and efficient way to combat the global warming issue and greenhouse effect. The viability of the CO_2RR critically rests with finding highly active and selective catalysts that can accomplish the desired chemical transformation. Single-atom catalysts (SACs) are ideal in fulfilling this goal due to the well-defined active sites and support-tunable electronic structure, and exhibit enhanced activity and high selectivity for the CO_2RR. In this review, we present the recent progress of quantum-theoretical studies on electro- and photo-chemical conversion of CO_2 with SACs and frameworks. Various calculated products of CO_2RR with SACs have been discussed, including CO, acids, alcohols, hydrocarbons and other organics. Meanwhile, the critical challenges and the pathway towards improving the efficiency of the CO_2RR have also been discussed.

1. Introduction

Due to the increasing fossil fuel combustion and energy consumption, carbon dioxide (CO_2) emission has led to serious global environmental problems such as global warming, sea level rising and ocean acidification.[1] The shortage of fossil energy has become a serious problem which needs to be solved urgently. Fortunately, it has been found that CO_2 can be used as a chemical feedstock to synthesize a variety of valuable chemical products or be converted into specific fuel substances such as methanol and methane. It will not only decrease the pressure on energy demand, but also reduce the amount of greenhouse gases.

Many efforts have been devoted to the conversion of CO_2 in recent years.[2–5] The electrocatalytic CO_2 reduction reaction (CO_2RR) has been widely applied for both industry and academia because of its high efficiency and activity.[6,7] The investigations normally focus on the electrochemical overpotential, current efficiency and products selectivity.[8,9] Nowadays, due to the requirement of energy regeneration and environment protection, photocatalysts have been paid more and more attentions because of the significance in the future applications of CO_2RR.[10–15]

The concept of single-atom catalysis (SACs), firstly proposed by Zhang, Li, Liu *et al.*,[16] has been widely used in heterogeneous catalysis,[17–20] which have shown the rosy prospects to achieve high activity, selectivity and ~100% atom utilization. From then on, it had developed preternaturally fast on enabling heterogeneous reduction products.[21–27] The CO_2^*– radical intermediate formed from CO_2 activation will affect the reaction pathways due to its instability and readily protonation, and further influence the activity and selectivity of electro- and photochemical reaction process. Some efforts have been taken to adjust the interaction between the intermediates and catalysts, such as improving the activities of catalyst surface and reaction environment.[28] For SACs, the unsaturated coordination can effectively regulate the relevance of CO_2 and correlative intermediates with particular active sites, which is promising for highly efficient CO_2RR catalysts.[29–31] However, the metal monatom has high surface energy that tends to aggregate particles with low surface energy during the reaction. Therefore, the preparation of stable SACs is still a great challenge. It has been proved that theoretical calculations methods such as density functional theory (DFT), molecular dynamics (MD) and Hartree–Fock (HF) are important for the data reliability. For instance, Qiu *et al.* revealed that Co–N_5 formed by inducing electron delocalization of Co–N_4 sites using nitrogen-rich carbon nitride as supporting material can improve the stability and conductivity by DFT calculations. The catalyst synthesized according to this prediction can remain for 40 h with excellent performance in CO_2 conversion to CO with >99% selectivity.[32] Metal–organic framework (MOF) materials, with periodic structure and designability of functional groups, have also been found an ideal carrier to stabilize metal monatom

[a]*School of Physics and Telecommunication Engineering, School of Materials Science and Engineering, Shaanxi Laboratory of Catalysis, Shaanxi University of Technology, Hanzhong 723001, China. E-mail: qiyu@snut.edu.cn*
[b]*Department of Chemistry and Key Laboratory of Organic Optoelectronics & Molecular Engineering of Ministry of Education, Tsinghua University, Beijing, China*
[c]*Guangdong Provincial Key Laboratory of Catalysis, Southern University of Science and Technology, Shenzhen 518055, China*

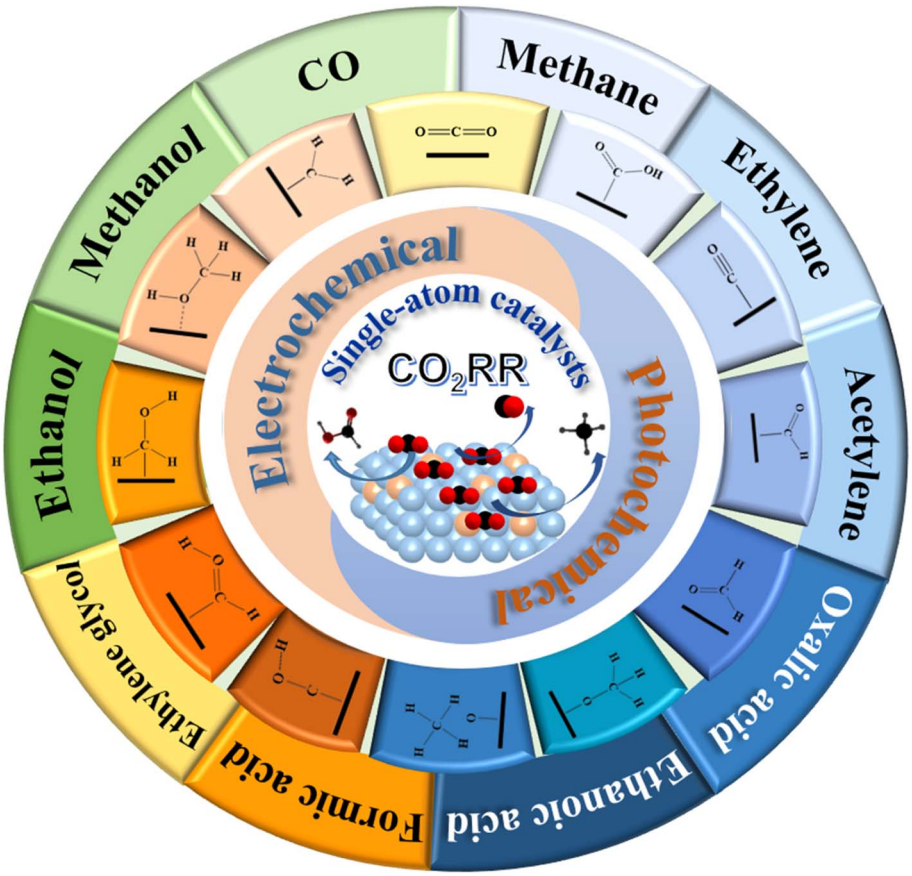

Fig. 1 The intermediate and final products of quantum-theoretical studies on electro- and photo-chemical CO_2RR with SACs.

when coordination chelating sites were introduced. Hai *et al.* summarized theoretical studies of MOFs, in which the performances of electrocatalysts for CO_2RR were involved. The MOFs showed the better catalytic performance than that in the respect of potential barriers, overpotentials, the energy barrier of C–C dimerization, selectivity and activity for CO_2RR.[33] Thus, it is promising to investigate CO_2RR with SACs from the perspective of theoretical calculations, which can guide the catalysts design. The intermediate products of CO_2RR include but not limit *COOH, *CO, *CHO, *OCH_2, *OCH_3, *COH, *CHOH, *CH_2OH, *CH_3OH, *CH_2 (as shown in Fig. 1). The reduction of CO_2 can generate CO, methane, ethylene, acetylene and other organics.

Above all, we need to provide an updated review to investigate the theoretical research on electro- and photo-chemical conversion of CO_2 with SACs. The framework is also described with reaction products, which will provide guidance for the experimental design of catalysts.

2. Electrochemical conversion of CO_2

In Electrochemical CO_2RR (eCO_2RR), electrocatalyst plays a key role because of its promising application on selectively synthesizing various C_1, C_2, and other polycarbonate compounds. However, the kinetics of eCO_2RR is limited due to the stable linear molecule structure of CO_2. At the same time, the transfer of multiple electrons and protons causes intricate final products, including HCOOH,[34] CO,[35] HCOH,[36] CH_3OH,[37] CH_4,[38,39] as well as competitive hydrogen evolution reaction (HER).[40] In order to improve the activity, selectivity and stability of the catalyst, the theoretical study on eCO_2RR can be commenced from two aspects, the design of the catalyst and the expand of the reaction mechanism.

At present, most of catalyst designs focus on the final products or reaction characteristics with different types of catalyst supports and active sites. It is proposed two strategies to improve: (1) increase the number of active sites; (2) enhance the intrinsic activity of single active site.[41] In addition, based on the theoretical calculations, the catalysts can be designed and predicted in microscopic level. The reaction energy barriers of intermediates for different catalysts are calculated to further investigate the reaction pathway and mechanism of CO_2RR.

2.1 eCO_2RR to CO

As one of the most fascinating conversion reaction methods, eCO_2RR to CO has attracted lots of attentions due to the Fischer–Tropsch (FT) type reaction.[42] Meanwhile, it's a key point to enhanced the selectivity for the eCO_2RR to CO in liquid environment.[43] Most of these works aimed at clarifying the reaction paths and selectivity trends, yet the mechanism of catalytic is still debatable which will not be further studied in

this paper. eCO_2RR to CO is a 2-electron reduction reaction consisted with two basic steps.[44] CO_2 reductively adsorbed on the surface of catalyst involved a proton coupled electron transfer process. As a result, *COOH intermediate is formed. The adsorbed intermediate further turned into *CO when another electron proton transfer, finally desorbed from the catalyst surface. Recently, SACs have been widely studied for eCO_2RR to CO because of its superior activity and selectivity compared with traditional catalysts. Table 1 summarizes the key parameters of eCO_2RR to CO with various SACs, including the reaction energy (ΔE) of the main steps, Faraday efficiency, over potential and max current density.

Besides, the single-atom metal-composite materials have exhibited unique properties in eCO_2RR. The metal centers dispersed atomically and coordination-unsaturated are favorable for providing active sites. Wang *et al.* synthesized a graphene-based Fe–N_5 SCAs as seen in Fig. 2a. The weak binding energy of CO is conducive to dissociation from the adsorption site of the catalyst. The valence electrons of Fe atom are reduced due to the axial pyrrole nitrogen ligand at Fe–N_5 site, which weaken the back donation from the 3d orbital of Fe atom to the π^* orbital of CO to realize the rapid desorption. High CO-selectivity is achieved as a result. Fig. 2b shows the diverse rate determining steps of Fe–N_4 and Fe–N_5 catalysts. The plane charge density by O–C–Fe–N (Fig. 2c) indicated the decrease of charge density of Fe atom. It confirms that the oxidation state of Fe in Fe–N_5 result in a weaker CO adsorption strength.[45] Deng *et al.* have doped different transition metals (Mn, Fe, Co, Ni and Cu) in the M–N_4 coordination phthalocyanine (MePcs). According to the results of DFT calculation (Fig. 2d), the rate determining steps for Co, Fe, and Mn reaction paths are the dissociation of *CO on the catalyst surface. But for Ni and Cu, the formation of *COOH exhibits the highest energy barriers among all the steps in CO_2RR. Fig. 2e describes the linear relationship between the adsorption energies of *CO and the reaction energies of CO desorption or *COOH formation. The two linear relations reveal an inverted volcano curve, and CoPc is the closest to the peak of volcano. Thus, the Co center in CoPc is the optimist reaction site by calculation. Fig. 2f shows the intermediate from CO_2 adsorption on the catalyst surface to the final continuous hydrogenation to CO*.[1] Cao *et al.* reported a method of anchoring atomically dispersed Co on polymer-derived N-doped hollow porous C spheres. The Co–N_5 plays a critical role in the CO_2 activation, *COOH formation and CO dissociation. Its catalytic activity is 15.5 times by CoPc.[46]

Meanwhile, adjusting the coordination number can effectively influence the catalytic activity of eCO_2RR. For instance, N-doped catalysts verified low coordination N could accelerate the formation of *COOH intermediate and promote eCO_2RR to CO with the theoretical calculations;[47] C-based SACs could exhibit low activation energy and favorable CO selectivity;[7] Pd–N_4 SACs also showed satisfactory reaction paths to the dissociation of CO.[48] Recently, Qiao *et al.* successfully synthesized a N-doped graphene supported Cu SACs (Cu–N_4-NG) which exhibited more favorable thermodynamics and kinetics than HER.[49] They further studied the electrocatalytic activity of 3d transition metal doped M–N_4–C (M = Mn, Fe, Co, Ni, Cu and Zn) catalysts for eCO_2RR.[67] Coincidentally, Lin *et al.* successfully prepared single atom Zn supported on NC nanofibers, and found that Zn–N_4 could effectively reduce the free energy barrier of *COOH.[50]

Table 1 The key parameters on eCO_2RR to CO with different SACs

SACs	ΔE (eV)	Faraday efficiency (%)	Overpotential (V)	Max current density (mA cm^{-2})	TOF (h^{-1})	Calculation method	Ref.
FeN_5	0.77	97.0	0.35	—	—	DFT	45
CoPc	−0.1	99	−0.8	—	—	DFT	1
Co–N_5	0.67	99.2	−0.73	4.5	480.2	DFT	46
Ni–N_3–C	0.66	95.6	−0.65	6.64	1425	DFT	47
Fe–N_4	0.94	86.5	−0.75	5	—	DFT	7
Pd–N_4	—	55	−0.5	—	—	DFT	48
Cu–N_4–NG	1.28	80.6	−1	—	—	DFT	49
Zn SAs/N–C	∼0.6	94.7	0.33	121.5	8190	DFT	50
ZnO@ZIF-NiZn	—	98	−1	34.3	9366	DFT	51
Cu–N_4	−0.9	96	−0.7	—	—	DFT	52
N–C–CoPc NR	−0.34	85.3	−0.7	30(0.18 V)	—	DFT	53
Co@Pc/C	0.89	84	−0.9	28	—	DFT	54
SA-Fe/NG	∼0.5	97	−0.5	—	—	DFT	55
Fe–N_4	0.29	94	0.58	4.59(−0.58 V)	1630	DFT	56
Fe–N/CNF	—	95	−0.53	4.71	3104	DFT	57
F-CPC	—	88.3	−1	37.5	—	DFT	58
Ni–N_4	0.89	98	−0.5	35.9(−1.35 V)	—	DFT	59
Ni/Fe–N–C	0.47	98	−0.7	23.7(−1.0 V)	7682	DFT	60
Ni–NG	0.12	95	0.55	50	2100	DFT	61
Ni–N–C	∼1.7	85	−1	200	—	DFT	62
Ni–SA–NCs	—	99	−0.8	50(−1.0 V)	—	DFT	63
Ni@NC-900	—	96	−1	−17	—	DFT	64
Ni–N@NPC	1.53	98.44	0.67	30.96	2825	DFT	65
NiPc–OMe	∼0.4	99.5	−0.61	−150	—	DFT	66

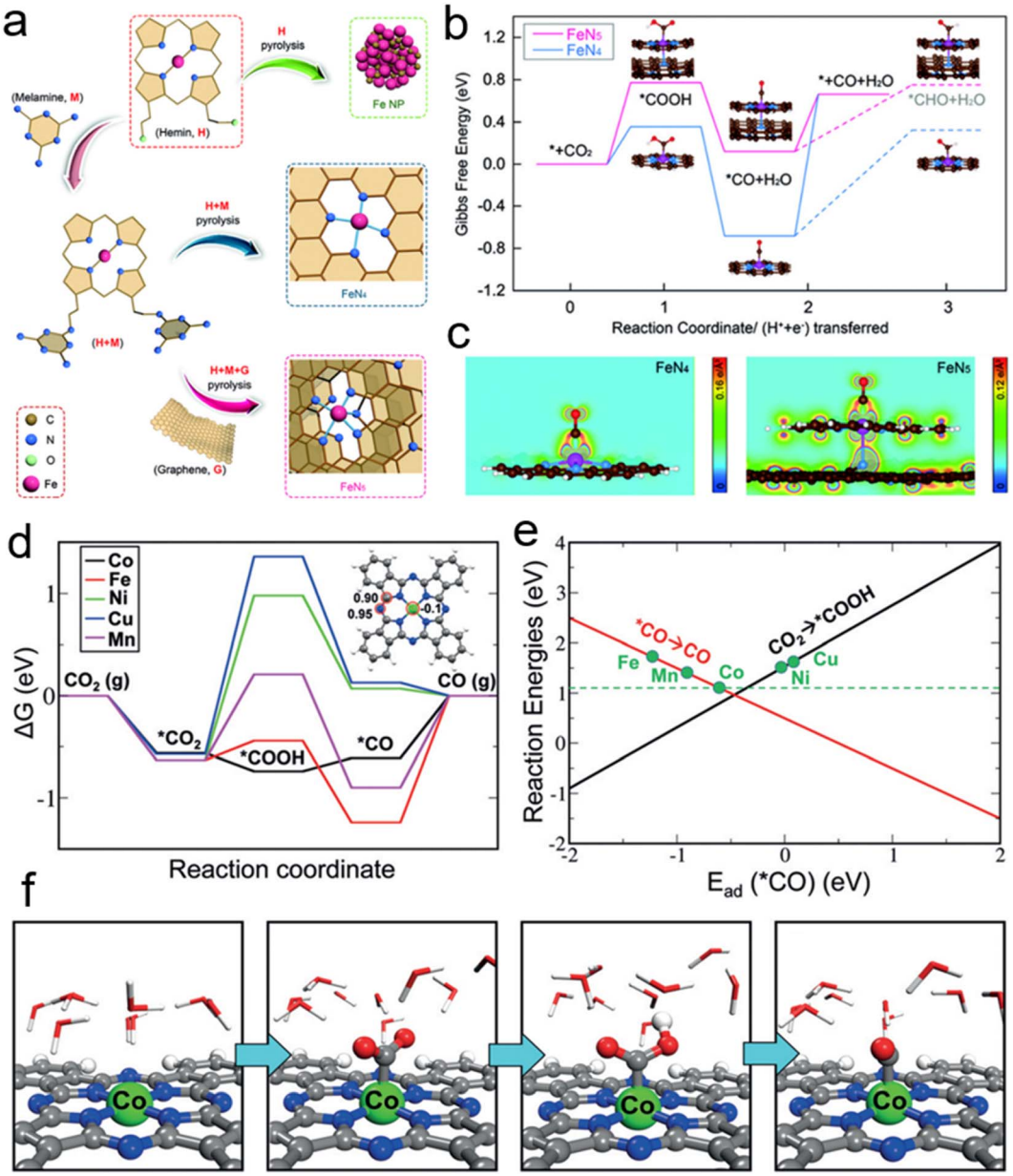

Fig. 2 (a) The structures of single-atom FeN_4 and FeN_5 catalysts. (b) The free energy of the optimized intermediate for the electroreduction of CO_2 to CO. (c) The plane charge density distribution of O–C–Fe–N. (d) The free energy of eCO_2RR on several SACs. Illustration shows the adsorption energy of *COOH. (e) CO dissociation and *COOH formation tendency of catalysts doped with transition metals. (f) The adsorption configurations of intermediates in liquid environment. The balls in green, blue, grey, red and white represent Co, N, C, O and H atoms, respectively (reproduced from ref. 1 with permission from John Wiley and Sons, copyright 2018; reproduced from ref. 45 with permission from John Wiley and Sons, copyright 2019).

Various Ni doped catalysts supporting have been extensively studied and demonstrated excellent performance in CO_2RR.[59–66] Wang *et al.* found that Ni–N@NPC with high dispersed Ni–N sites and desirable CO_2 adsorption capacity exhibited high faradaic efficiency for CO (about 98.44%) and durable stability over 30 hours. The eCO_2RR activity was indicated by DFT calculation which revealed that Ni–N sites can decrease the kinetic energy barriers for *CO_2 to *COOH.[65] Sun *et al.* reported a thermodynamically stable Ni single atom with a Ni–N_3 structure and further wrapped in porous N-doped C shell. The free energy barrier for *COOH on Ni@N_3 is much lower than that of Ni@N_4.[68]

Moreover, Han *et al.* successfully prepared N, P-co-doped carbon aerogels, which could be used as electrocatalysts to efficiently reduce CO_2 to CO. With high active area and conductivity, it provided a promising approach for non-metallic catalysts.[69] Fig. 3a shows the configuration of N-/P-doped, and N, P-co-doped carbon. As shown in Fig. 3b, the free energy barrier is significantly reduced after doping with heteroatoms. Among them, the pyridinic N exhibited the lowest

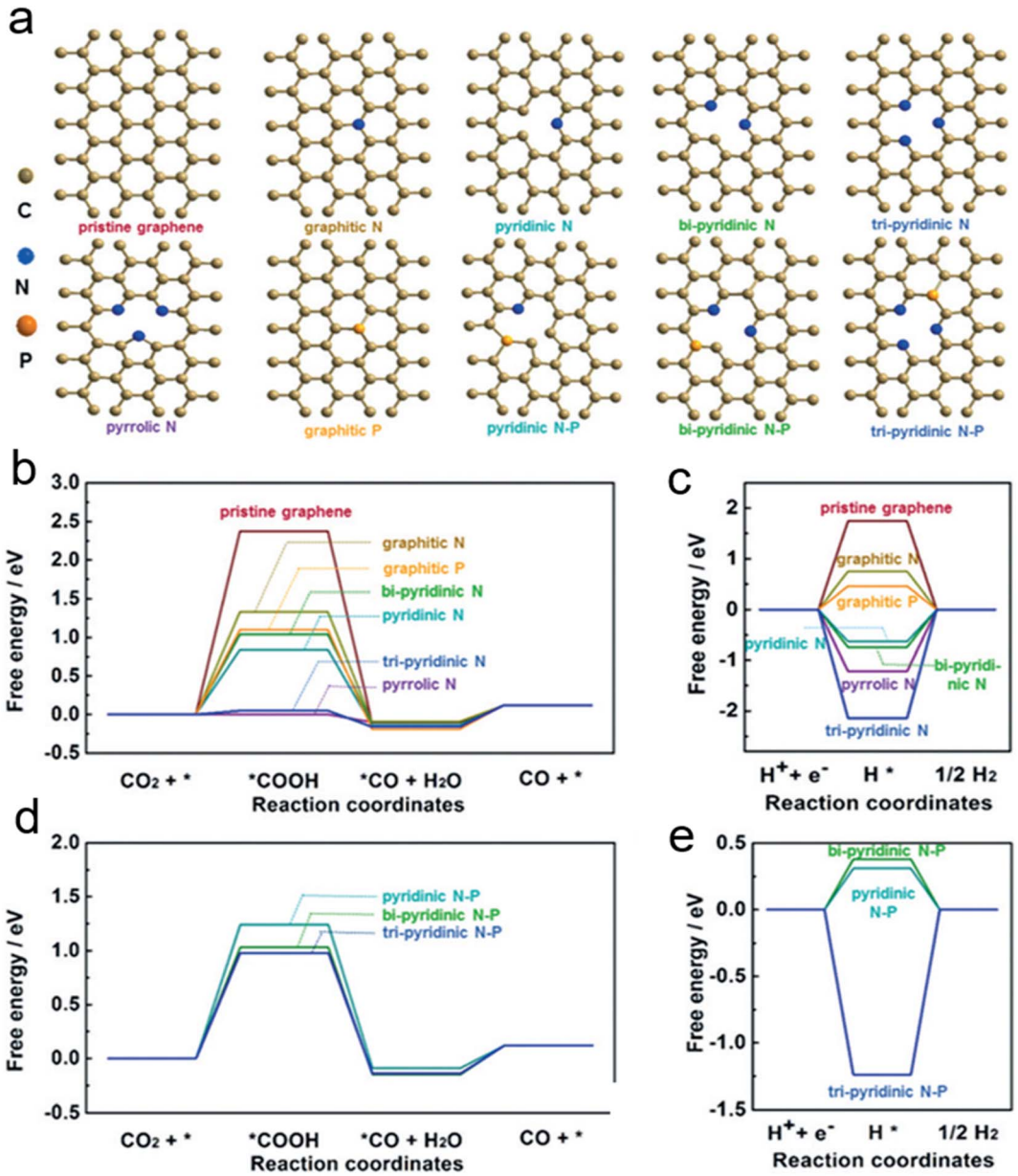

Fig. 3 (a) A series of N/P-doped, and N, P co-doped carbon configurations. (b) Gibbs free-energy (ΔG) diagrams for eCO_2RR to CO. (c) ΔG for HER. (d) ΔG for eCO_2RR to CO based on N, P-co-doped carbon. (e) ΔG for HER based N, P co-doped carbon (reproduced from ref. 69 with permission from John Wiley and Sons, copyright 2020).

free energy barrier. Besides that, the adsorption of H* on both tri-pyridinic N and pyrrolic N is strong from the HER free energy in Fig. 3c. Thus, the pyridinic N is the active site in eCO_2RR to CO. Moreover, the free energy changes of eCO_2RR and HER on carbon Co doped with N–P were also calculated (Fig. 3d and e). N, P-co-doped carbon aerogels have considerable activity and selectivity for the eCO_2RR to CO. Furthermore, they synthesized Sn_4P_3/reduced graphene oxide nanocomposites and Cu–Co bimetallic nanoparticles which exhibited excellent catalytic activity and selectivity of eCO_2RR to CO.[70–72]

In addition, eCO_2RR is thermodynamically more favorable compared with HER. For instance, N-doped carbon catalyst with Ni sites can exhibit nearly 100% CO selectivity and high activity.[51] Atomically Fe^{3+} site facilitate high-efficiency CO_2 electroreduction catalysis which catalyze eCO_2RR to CO under a low overpotential. Zn supported on N-doped carbon catalyst can inhibit the generation of CO and increase the selectivity of CH_4.[29] Except for the use of carbon-based materials as the catalyst carrier, boron nitride is similar to graphene and has excellent physical and chemical properties. Therefore, transition metal-doped BN nanomaterials have been investigated in eCO_2RR with SACs. Transition metals (TM = Sc to Zn, Mo, Ru, Rh, Pd and Ag) are doped on BN monolayers. The DFT calculation present that monoatomic TM–BN have excellent catalytic performance as catalysts for reducing CO_2 to CH_4.[73]

In recent years, the single atom alloy has developed catalytically active element composed of atoms dispersed in host metal with high catalytic selectivity. This catalyst combines the traditional advantages of alloy catalysts with the new features of SACs. The adsorption energy of *CO corresponds to the theoretical overpotential of methane or methanol, so as to achieve the screening of high-performance catalysts,[74] further effectively reduce the activation barrier of CO_2.[75] The weak binding energy of CO greatly reduces the possibility of catalyst poisoning and further protonation, leading to perfect CO selectivity and stability.[76]

2.2 eCO_2RR to alcohols

Another strategy to reduce CO_2 is to generate safe and transportable liquid fuels. Alcohols has become an attractive product due to its core position in the fields of national defense, industry and agriculture.[77] However, because of the complex reaction intermediates, high energy barrier and complicated mechanism of C–C coupling, the selectivity of alcohols is not optimistic.[78]

By reducing the size of metal-based catalysts to single atom level,[79,80] Wang *et al.* successfully prepared cobalt atom electrocatalysts/nanoparticles and carbon/selenium on N-doped porous carbon (Co_{SA}–HC, Co_{NP}–HC, Se@Co_{SA}–HC, respectively). The catalyst exhibits distinguished coulombic efficiency, high reaction rate and strong stability. Fig. 4a shows the synthetic schematic diagram of Se@Co_{SA}–HC, which is inserted selenium into carbon particles with hollow structure. The intermediate and free energy changes after structural optimization are observed in Fig. 4b. The transformation of Se_8^*, $Li_2Se_8^*$, and $Li_2Se_6^*$ are exothermic process, while $Li_2Se_4^*$, $Li_2Se_2^*$ and Li$_2$Se* are endothermic. In addition, the free energy of reaction of $Li_2Se_2^* \rightarrow Li_2Se^*$ on Co–NC is lower than that of NC, which exhibits thermodynamically more favorable for the reduction of Se. By calculating the phase change barriers of $Li_2Se_2^*$ on Co–NC and NC (Fig. 4c and d), Co atoms are the active center of the catalyst.[81] In addition, SACs with uniformly dispersed active metal centers are highly unsaturated coordinated and exhibit quantum confinement effect,[82] resulting in a high electron density distribution near the Fermi level, which contributes to the rapid electron transfer in the catalytic reaction process.[83,84] MXene anchored SACs by selectively etching hybrid A layers (Al and Cu) for eCO_2RR have been studied by DFT calculation. The monoatomic Cu with unsaturated electronic structure effectively reduces the energy barrier of the rate determining step. The rate determining step of the reaction path is the conversion of HCOOH* to the intermediate of adsorbed CHO*, which was helpful for eCO_2RR to CH_3OH. As shown in Fig. 4e, through the charge density difference of SACs–Cu–MXene, Cu has a positively charged Cu–O_3 structure and the designed reaction path. Based on DFT calculations (Fig. 4f), SACs can significantly reduce the reaction barrier of eCO_2RR.[85] Co@Cu SACs would also exhibit ideal performance in converting CO_2 to CH_3OH. The narrowed Co d-band stabilizes the adsorption of CO_2 on the surface and further enhances the bonding of COH* to the active site. While stabilizing the intermediate, it reduces the activation energy of COH* for further hydrogenation. It effectively prevents the C–C coupling and enhanced the selectivity of the reaction to CH_3OH.[9]

Various efforts have been made on reducing the activation energy to promote eCO_2RR to CH_3OH. The normal reaction path for calculation is $*CO_2 \rightarrow *CO \rightarrow *CHO \rightarrow *CH_2O \rightarrow *CH_2OH$ and $*CH_3O \rightarrow CH_3OH$.[86] It could significantly enhance CO_2 protonation ability by reducing the distance between adjacent monomers and catalysis.[87] By DFT calculations, Ding *et al.* have discovered that TM (TM = Fe, Co, Ni, Cu, Ir and Pt) could effectively improve the catalytic activity and enhance the redistribution of electrons. Besides that, they could further activate the subsequent reaction intermediates, and finally selectively generate CH_3OH.[88]

The instability safety limits the reserves of precious metal catalysts, which is the obstruction of industrial production, as well large-scale preparation. In addition, the stability is also an insurmountable gap for non-precious metals. Meanwhile, lots of attempts have been researched on metal catalysts, the main advantages of which catalysts are low overpotential, high current density, large specific surface area and less metal consumption. Cobalt phthalocyanine could be immobilized on carbon nanotubes to selectively catalyze eCO_2RR to CH_3OH. The electrocatalytic reaction followed domino process: $CO_2 \rightarrow CO$ by two electrons, $CO \rightarrow CH_3OH$ by four electrons.[89] Meanwhile, TM dimer doped on graphene with adjacent single vacancies could reduce overpotential and enhanced current density in eCO_2RR, which further improve the catalytic performance.[2] By constructing the network inter-perforation and self-supporting structure, the probability of single atoms at the interface is greatly increased, high current density can be achieved at a lower metal single atom content as a result, which has certain practical application prospects.[90] Besides that, new materials including 2D, 0D, and Janus material have been found to be promising as efficient electrocatalysts for eCO_2RR. For instance, Chen *et al.* have developed tricycloquinazoline based 2D c-MOFs successfully, which showed high selectivity toward CH_3OH with Faradaic efficiency up to 53.6%. The eCO_2RR performance is even better than Cu- and MOFs-based electrocatalysts.[91]

In recent years, ethanol with higher energy density as an ideal fuel has also been a research hotspot.[92] Copper clusters supported by catalyst had a mixed charge state of Cu^0 and Cu^{x+}. The coverage of *CO on the surface was increased, making it possible to couple C–C on the Cu_t^0–Cu_b^{x+} atomic interface, and finally generated C_2H_5OH.[93] The construction of dual active sites by loading single atom on carrier provided a new attempt for the design of the catalyst through the synergistic effect of the single-atom center and substrates.[94]

At present, the design strategies of CO_2 to alcohols monatomic catalysts mainly include by SACs in covalent organic frameworks. However, due to the complicated intermediates and reaction pathways, the mechanism of eCO_2RR is still ambiguity. Meanwhile, varieties of by-products will be generated in the related reaction path. The reasonable design of the carrier, the regulation of the reaction conditions, and even the

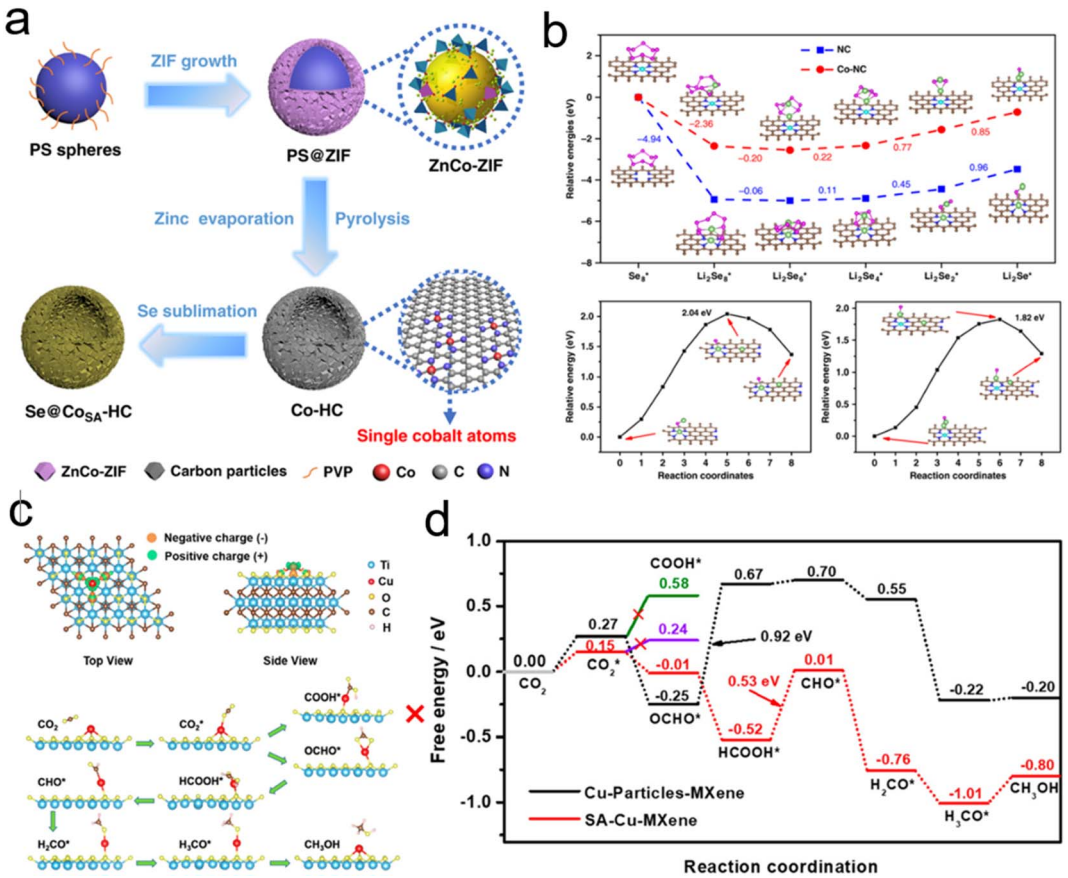

Fig. 4 (a) Schematic of Co/N doped hollow porous carbon. (b) The energy distribution of Li_2Se compounds/cluster reduction on NC/Co–NC carriers. (c) The charge density of SACs–Cu–MXene. The green/orange area indicates the increase/decrease in electrons. The reaction path for the eCO_2RR to CH_3OH. (d) The free energy change trend of eCO_2RR to CH_3OH (Reproduced from ref. 81 with permission from Springer Nature, copyright 2020; reproduced from ref. 85 with permission from American Chemical Society, copyright 2021).

structure of the carrier are all significant effects on the selectivity of products.

2.3 eCO_2RR to acids

Formic acid is one of the basic organic chemical raw materials. It is widely used in the industry of pesticide, leather, rubber, dyestuff and so on. It also has the potential application for hydrogen storage and fuel cells.[95] In addition, formic acid is also an indispensable intermediate for the synthesis of higher alcohols. In fact, CO_2 and H_2 can generate formic acid relatively easily except the kinetic obstacles of reaction process that need to be resolved.[96] Therefore, it is very necessary to find suitable, efficient and stable catalysts.

As a very ideal electrocatalyst, indium (In) can efficiently reduce CO_2 to formic acid, but it cannot be further promoted because of the high potential and low FE. In SACs based on N-doped carbon matrix derived from the metal–organic framework have found to be excellent in this regard. The catalyst has well-dispersed $In^{\delta+}$–N_4 atomic interface sites, which can efficiently catalyze eCO_2RR to formic acid. $In^{\delta+}$–N_4 atomic interface has lower free energy for the formation of intermediate HCOO*, which is beneficial to improve the catalytic activity for eCO_2RR. It provides a feasible strategy for precise adjustment of indium catalysts at the atomic level for efficient eCO_2RR.[97] Meanwhile, TM (TM = Sc, Ti, V, Cr, Mn, Fe, Co, Ni, Cu and Zn) SACs can stably be supported on porphyrin framework. This new catalyst designed strategy on eCO_2RR to acids provides a different enlightenment for experimental design.[21] Hai *et al.* found that, for some MOFs, the selectivity of HCOOH depended on the adsorption energy difference between *HCOO and *COOH by DFT calculations.[98] Thus, the biggest obstacle is that HER would severely inhibit eCO_2RR.[99]

Graphite carbonitride (g-C_3N_4) contains unique chemical composition, π-conjugated electronic structure and strong nucleophilic ability. Thus, it can be used as multifunctional catalyst in traditional organic catalytic reaction, such as green carrier and energy storage material. Based on first-principles calculations, systematic studies have been carried out on the geometric configuration, electronic structure and eCO_2RR catalytic performance of graphdiyne-supported alkali metals which had great potential as SACs for eCO_2RR. The conversion mechanism by constructing model of S-doped Cu has been calculated, which could effectively enhance the adsorption strength of *CO to further selectively generate HCOOH,[100] as well as Ru SACs on layered double hydroxide.[101] low-

coordination active center and oxygen vacancies could selectively generate HCOOH while inhibiting HER.[102]

The heterogeneity of the catalyst support surface limits the further development of SACs, including synthesis and catalytic performance. In recent years, SACs have begun to construct active centers at the molecular level to improve the stability of the active centers and realize the "quasi-homogeneous" application. Zhang *et al.* successfully prepared a porous organic polymer containing pyridine-amide groups with Ir SACs on the porous organic polymer. It exhibits excellent catalytic activity in the CO_2RR to formic acid with excellent cycle stability. The SACs have the same catalytic reaction mechanism as the homogeneous catalysis process.[103] The solid micelle can increase the number of active sites of the carrier species, meanwhile, the reaction conditions are more tolerant, and the product can be easily separated.[104]

2.4 eCO$_2$RR to other organics

In addition to C_1 and C_2, the products of eCO$_2$RR also included olefins,[105] alcohols, ketones,[106] aldehydes,[107] and even C_3 and C_4 products.[108] Compared with the C_1 product, the multi carbon products have more considerable energy density. Moreover, multi carbon products play an important role in the chemical industry.[109] Ethylene is a basic raw material for the synthesis of plastics, rubber, fiber and ethanol, which occupies an important position in the petrochemical industry. However, eCO$_2$RR to C_{2+} also faced with the obstacles of C–C coupling complex process, as well as the problem of adsorbate coverage on the surface.

CO_2 can be adsorbed on the surface with strong adsorption strength. Metal doped catalysts could show high selectivity and activity for the formation of CH_3OH.[110] Fig. 5a and b show the possible reaction pathway about C_1 and C_2.[111] Recently. The reaction mechanism of C_2H_4 was studied by constructing asymmetric.[112] Cu/C can significantly promote coupling and maintain a moderate binding energy between the intermediate and the carrier.[113] For instance, Cu–C_3N_4 has been studied on the adsorption behavior of intermediates in the eCO$_2$RR process. The catalyst can effectively reduce the onset potential with excellent catalytic activity. The generation rate of C_2 is significantly better than that of Cu–NC.[114] The excellent selectivity for C_2H_4 on the Cu-based MOFs for eCO$_2$RR has been

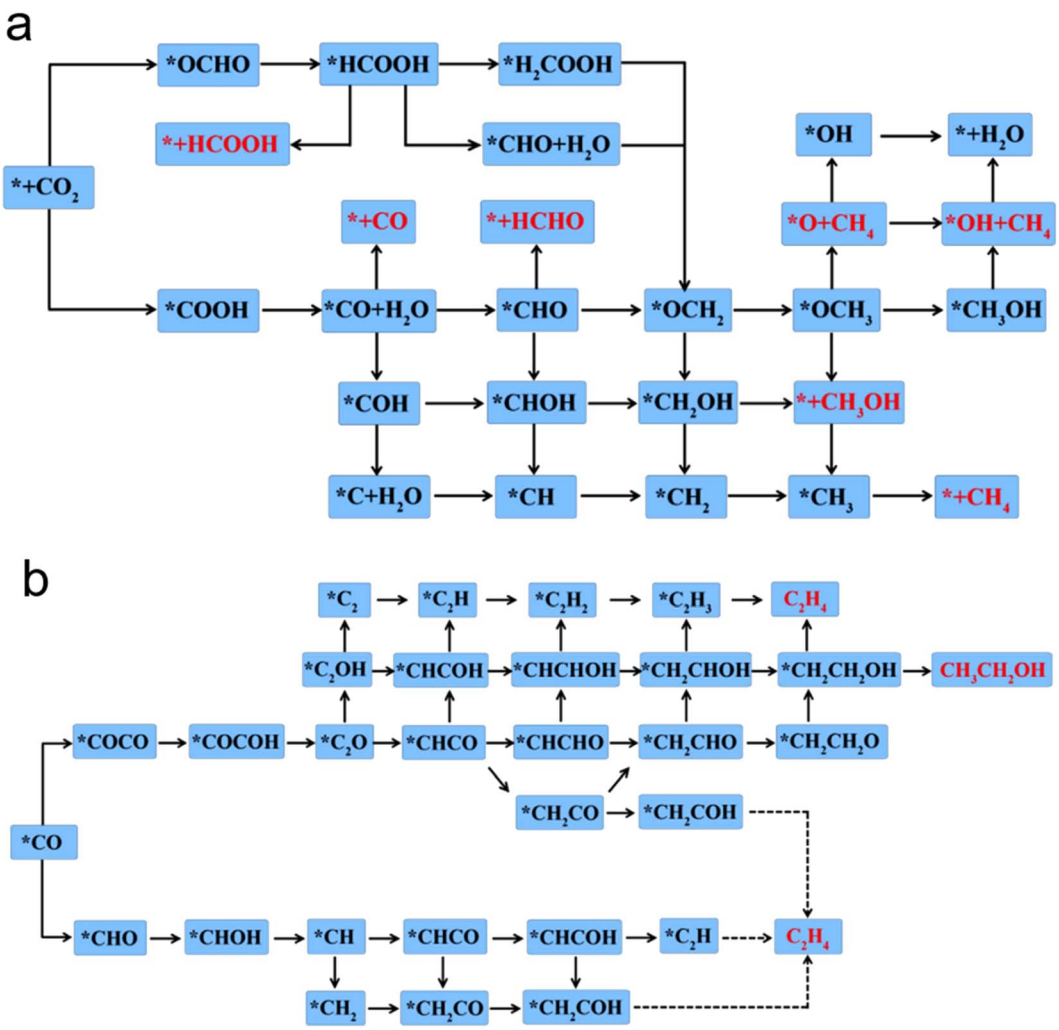

Fig. 5 The eCO$_2$RR reaction pathways to (a) C_1 products and (b) C_2 products on Cu_2@CN catalyst (reproduced from ref. 111 with permission from John Wiley and Sons, copyright 2020).

reported by Yang *et al.* with isolated Cu–S motifs in MOF based precatalysts.[115] At present, the C_3 and C_4 products have also begun to arouse widespread concern on multi-carbon products. Dismukes *et al.* synthesized nickel phosphide compounds, which were used to reduce CO_2 in aqueous solutions and studied the catalytic performance of eCO_2RR. The product selectivity has a significant change by increasing the phosphorus content. They proposed a reaction pathway for the efficient synthesis of multi-carbon products from CO_2 through formic acid and formaldehyde intermediates without CO intermediates.[108]

Although lots of works have been done on eCO_2RR in recent years, most of them only stayed in the laboratory stage. How to find the catalyst with high efficiency and selectivity becomes a challenge.[116] Besides, most of the current catalyst designs have limitations due to that CO_2RR has complicated reaction paths and produces intermediates.[117] In addition, there is still lack of clear reaction mechanism. Many obstacles need to be overcome for SACs with excellent performance to be promoted and applied to industrial production.[118] Above all, based on what has been achieved so far, we believe that there will be a qualitative breakthrough in the practicality of eCO_2RR in the future.

3. Photochemical conversion of CO_2

Investigating photochemical CO_2RR (pCO_2RR) with SACs is a pressing environmental issue due to the increasing concentration of CO_2 in the atmosphere. Since Inous *et al.* first reported pCO_2RR to organic compounds in gas–solid reaction systems, a great deal of researches have been devoted to the development of photocatalysts for pCO_2RR.[11] Photocatalysts mainly include the following types: (1) metal oxides, mainly composed of d^0 structured (Ti^{4+}, Zr^{4+}, Nb^{5+}, Ta^{5+}, W^{6+}, and Mo^{6+}) and d^{10} (In^{3+}, Ga^{3+}, Ge^{4+}, Sn^{4+}, and Sb^{5+}) metal cations,[12,119] such as TiO_2, ZrO_2. $XTaO_3$ (X = Li, Na, K), $InVO_4$, $ZnGa_2O_4$, *etc.*;[120–125] (2) metal sulfides such as XS (X = Cd, Zn);[126–129] (3) metal nitrides such as GaN,[130] TaON;[131] (4) layered metal hydroxides (referred to as LDH), such as FeNi-LDH/g-C_3N;[132] (5) metal organic framework materials (MOFs), such as MOF-525-Co;[133] (6) non-metallic semiconductors, such as g-C_3N_4,[134] and graphene.[135]

Moreover, metal oxides,[16,136–138] MOFs,[139,140] C-based materials,[141,142] and LDH[143,144] are the common carriers for SACs. It has been reported that TiO_2,[145–147] CeO_2,[148,149] MOFs,[150–152] graphene,[153,154] graphitic carbon nitride,[155–157] LDHs[158,159] have shown high activity, stability and selectivity in pCO_2RR. The strong interaction between the single metal atom and the carriers is beneficial to improve the catalytic performance. Meanwhile, the application of pCO_2RR with SACs is an effective way to improve the rate of photocatalysis and achieve carbon emission reduction.

However, the high recombination rate of electrons and holes, the narrow wavelength-range of light to achieve the exited state, and the small specific surface area of conventional semiconductor photocatalysts limit the catalytic rate.[160,161] The photocatalytic performance of catalysts can be improved by co-catalysts and the noble metals, for example that Pt and Pd, are considered to be efficient co-catalysts.[162,163] The high cost and low abundance of precious metals limited the industrial application. Therefore, large specific surface area, stability, high selectivity, ability to inhibit recombination are the critical issues to design practical photocatalysts.[164–166]

Single-atom photocatalysts are photoactive materials in which metals are present as SACs uniformly dispersed on the support. The catalytic performance of SACs depends largely on the interaction between the support and metal.[167] For single atom photocatalysts, the introduction of SACs can effectively inhibit the electron–hole recombination, as well as increase the activity and selectivity.[168,169] The favorable SACs dispersion effect and prevention of metal SACs aggregation play important roles in the final catalytic activity of monoatomic photocatalysts. CO_2RR with SACs is a promising strategy for the conversion of CO_2 to hydrocarbon fuels such as CO, CH_4, and CH_3OH.[13,168,170]

The pCO_2RR requires the following steps (Fig. 6): (1) the photocatalyst is irradiated by light. It leads to the excitation of electron from valence band to conduction band, leaving a hole in the valence band, which is the photo-electron/hole pair;[171] (2) the photogenerated electrons and holes diffuse and separate. The electrons/holes transfer to the reduction/oxidation sites, respectively; (3) CO_2 is adsorbed onto the surface; (4) a redox reaction occurs on the photocatalyst surface, where the electrons reduce CO_2 to CO,[172,173] CH_4,[169,174,175] HCOOH,[176–178] CH_3OH[179–181] or other hydrocarbons,[170,182,183] and the holes oxidize water to molecular O_2 by cavities;[152,154,184] (5) products desorbed from the catalyst surface. The pCO_2RR and potentials are also exhibited. Fig. 7 shows the band edges commonly used in photocatalysts.[185] In this section, we summarize the theoretical studies of SACs in pCO_2RR, including CO_2 to CO, methane, and CH_3OH.

3.1 pCO_2RR to CO

Based on the thermodynamic principle of proton-assisted multi-electron transfer to reduce CO_2, the specific pathway for CO_2 reduction to CO is: $CO_2 + 2H^+ + 2e^- \rightarrow CO + H_2O$,[168,184,186] for pCO_2RR relative to the Normal Hydrogen Electrode (NHE) in aqueous solution.[187] The potential level of the conductive band of the photocatalyst determines the production of pCO_2RR.[188] In order to overcome the slow thermodynamic process and promote the reaction rate, the potential (*vs.* NHE) of the conduction band needs to be more negative than the reduction potential of CO_2. The energy band structure of semiconductor photocatalysts is extremely important for the catalytic efficiency. How to abbreviate the residence time of CO on the catalyst surface and accelerate the desorption from the catalyst surface into the gas phase are the key points to improve the catalyst selectivity.[189–191] The energy band structure of conventional semiconductor catalysts is far from ideal. In recent years, many researches have been conducted to improve the photogenerated electron–hole separation efficiency of photocatalysts by modifying the semiconductors to increase the light absorption rate and enhance the CO_2 adsorption capacity.

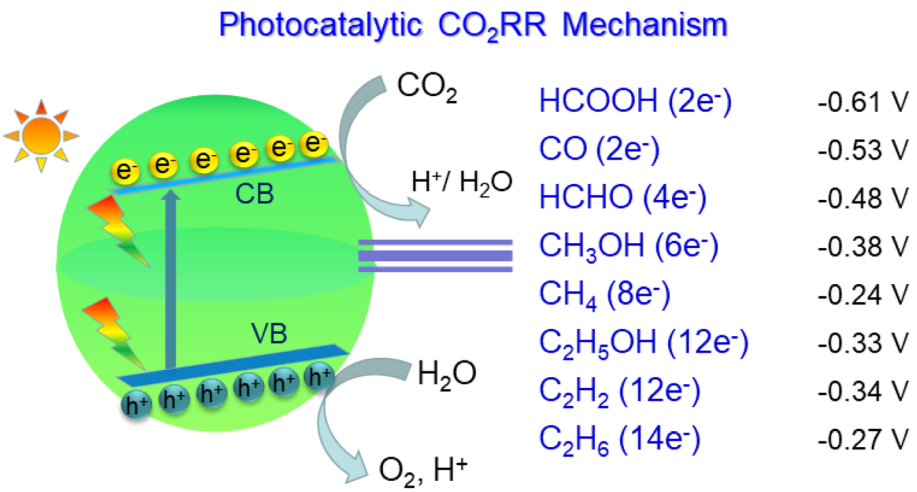

Fig. 6 The mechanism and steps of pCO_2RR. Including the electrons and reduction potential required for the pCO_2RR to different products with respect to the standard hydrogen potential NHE at pH 7.

The combination of monatomic transition metals and polymeric carbon nitride has been an effective strategy for photocatalytic reactions. Li *et al.* reported the preparation of copper carbon nitride nanocatalysts (Cu–CCN) based on the doping of monatomic Cu into CN by molten salt and reflux methods to promote the photoreduction of CO_2 to CO.[192] Density functional theory calculations further clarified the mechanism of the pCO_2RR process (Fig. 8a), where the CO_2 adsorbed on the surface of the Cu–CCN catalyst was hydrogenated to *HCOO, *CO, successively. And CO desorbed from the surface, finally. Wang *et al.* analyzed the mechanism of CN-loaded Cu single-atom pCO_2RR using DFT and found that the active center in the form of C–Cu–N_2 not only promoted charge transfer but also reduced the energy potential energy for pCO_2RR (Fig. 8b).[165] Meanwhile, Ji *et al.* reported an atomic confinement and coordination design strategy applied to design various metal monatomic catalysts.[193] Er monatomic catalysts (Er/CN-NT) loaded on carbon nitride nanotubes with tunable metal dispersion density were synthesized for pCO_2RR. According to the computational hydrogen electrode (CHE) model, it is confirmed that the favorable production is CO, instead of CH_4 on rare-earth erbium atom catalysts.

In addition to the above-mentioned design photocatalyst strategies, we have continuously developed single-atom photocatalyst design strategies that favor adjustable metal atom coordination and demonstrated their catalytic effects on the pCO_2RR to CO. Zhong *et al.* synthesized Ni-rich single-atom 2,2′-bipyridine covalent organic frameworks of photocatalyst (Ni-TpBpy) (Fig. 8c and d).[194] Ni-TpBpy was effective in improving the selectivity of CO generation in aqueous solution. Ni atom was stabilized by the dipyridine coordination unit based on the special structure. The hydrogen bonding between ketone node and Ni–CO_2 reaction intermediate promoted the pCO_2RR preferential to H_2 formation. Meanwhile, the adsorption of CO_2 by Ni-TpBpy was greatly improved due to the Lewis acid–base interaction between the loaded Ni ions and absorbed CO_2 molecules. DFT calculations used to investigate the mechanism for pCO_2RR confirmed that Ni-TpBpy could reduce the CO_2

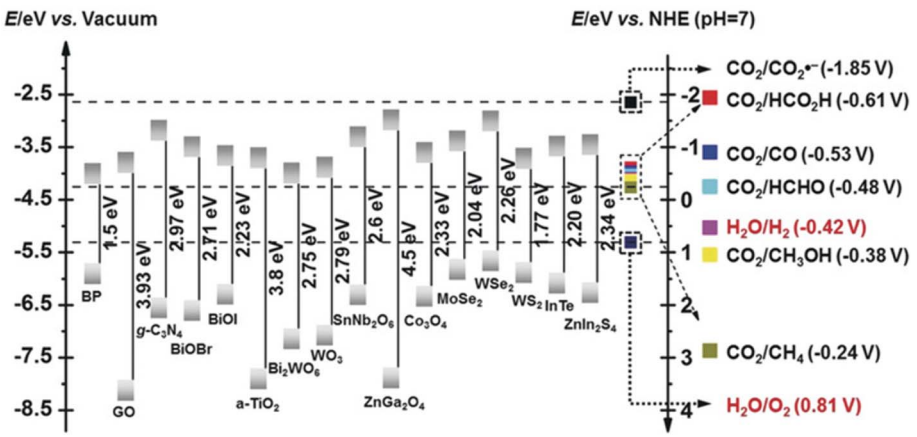

Fig. 7 CB and VB potentials of common semiconductors with CO_2 and water redox couples at PH 7 (reproduced from ref. 185 with permission from John Wiley and Sons, copyright 2018).

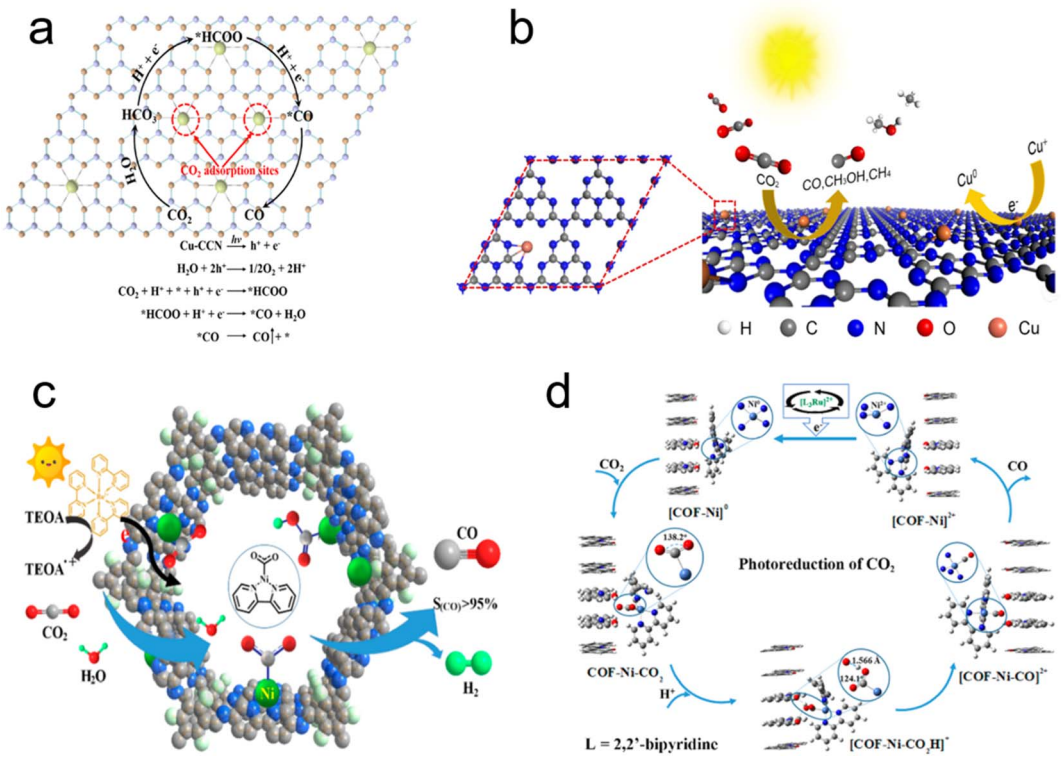

Fig. 8 (a) Schematic of the tentative photocatalytic mechanisms and reaction pathway of Cu–CCN for pCO_2RR. (b) Schematic illustration of Cu/CN hybrid for pCO_2RR. (c) Photocatalytic selective CO_2RR on Ni-TpBpy. (d) Proposed reaction mechanism for the photoconversion of CO_2 into CO on Ni-TpBpy (reproduced from ref. 192 with permission from American Chemical Society, copyright 2020; reproduced from ref. 165 with permission from American Chemical Society, copyright 2020; reproduced from ref. 194 with permission from American Chemical Society, copyright 2019).

molecules and activate Ni site to Ni–COOH, which would combine with H^+ to Ni–CO intermediate, followed by CO desorption from Ni–CO. Oxygen vacancies, as common defects in oxides or hydrogens carbide surfaces, has a great impact on pCO_2RR.[195,196] For instance, CO production rate of Co–Bi_3O_4Br was approximately 4 and 32 times than atomic layer Bi_3O_4Br and bulk Bi_3O_4Br.[164] Ni atoms could occupy the oxygen vacancies of ZrO_2, efficiently achieved pCO_2RR to CO, which is 6 and 40 times by that of defective ZrO_2 and complete ZrO_2, respectively.[63] Chen *et al.* have studied the adjustable catalytic performance and the modulation mechanism of Ni^{2+} doped NH_2-MIL-125-Ti (NH_2-MIL-125-Ni_x/Ti) with different Ni^{2+}/Ti^{4+} molar ratio (x = 0.5–1.5%) *via* an *in situ* doping method. They found that Ni around O atoms of Ti oxo clusters of NH_2-MIL-125 can change the electronic structure of the clusters thus lead to the improvements of electron transfer and charge separation. The highest CO_2 conversion rate with 98.6% CO selectivity was exhibited with the molar ratio 1%.[197]

So far, researchers have focus on using atomic confinement strategy, coordination design strategy, and defect engineering strategy to increase the active sites with CN, metal–organic backbone, and photocatalysts of monatomic metal to achieve improving photocatalytic activity. Thus, the pCO_2RR still have the obstacle in accelerating the rate of CO desorption, which is also the key to improve photocatalytic selectivity. So, it is also challenging to improve the CO_2 photoreduction activity and product selectivity.

3.2 pCO_2RR to CH_4

CH_4 is the main component of natural gas. Due to the limited petroleum resources, it will be a high-quality gas candidate fuel. pCO_2RR to CH_4 requires 8-electron reduction: $CO_2 + 8H^+ + 8e^- \rightarrow CH_4 + 2H_2O$.[198] The CO_2 molecule is very inert, which limits the catalytic conversion. At the same time, the products of CH_4 are frequently accompanied by CO and H_2, so that the efficiency and selectivity will be influenced. Thus, how to improve the quantum efficiency and increase the selectivity of pCO_2RR become the key issue for photocatalysis.

Zhang *et al.* realized the modular optimization of the metal–organic framework by injecting monoatomic Co SACs on porphyrin,[133] so as to synthesize the catalyst with atom dispersion (Fig. 9a). The catalyst significantly improves the electron–hole separation efficiency of the porphyrin unit and the CO_2 adsorption capacity, which realize the directional migration of photo-excitons from the porphyrin to Co center. It provides long-lived electrons for CO_2 molecules adsorbed on the Co center. The addition of unsaturated Co SACs achieves the enhancement of pCO_2RR, thus, greatly improves the selectivity of CH_4.

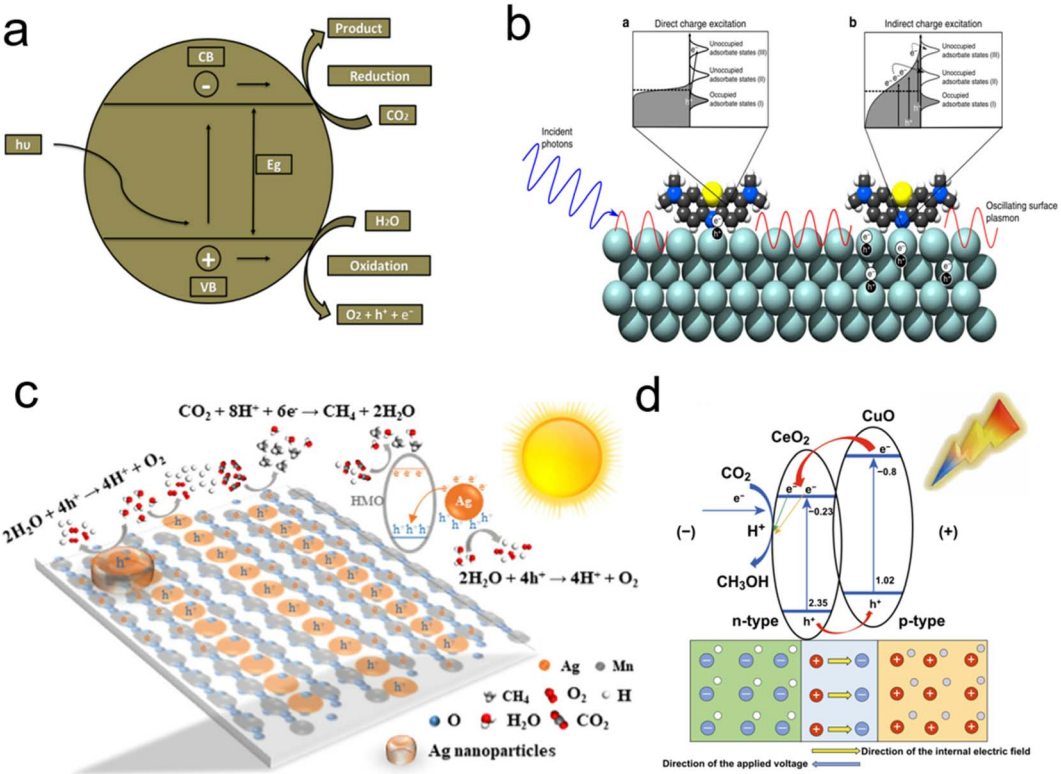

Fig. 9 (a) Schematic representation for construction of Cu-based ZIF catalyst and representation of pCO_2RR; (b) illustration of LSPR-mediated charge excitation mechanisms; (c) pCO_2RR mechanisms of Ag-HMO; (d)Proposed mechanisms for PEC pCO_2RR on the CeO_2 NPs/CuO NPs composite catalyst (reproduced from ref. 133 with permission from MDPI, copyright 2018; reproduced from ref. 199 with permission from Springer Nature, copyright 2016; reproduced from ref. 200 with permission from Elsevier, copyright 2019; reproduced from ref. 201 with permission from Springer Nature, copyright 2020).

Due to the heat generated by surface plasmon resonance of noble metals, the excited electrons can be easily transferred into the conduction band of the semiconductor,[202] which could facilitate the separation of electrons and holes to increase pCO_2RR to CH_4. Liu *et al.* reported Au–Cu alloy catalysts which was adjusted the structure of co-catalysts and improved the electron capture capacity.[203] Meanwhile, the $A_3Bi_2I_9$ ($A^+ = Rb^+$, Cs^+, CH_3NH^{3+}) were synthesized by Bhosale *et al.*,[204] which has shown excellent photocatalytic activity for pCO_2RR at the gas–solid interface. Besides, precious metal catalysts such as Ag, Au, and Pt loaded on metal-catalysts as SACs can effectively increase photoactivity. Ag nanoparticles were widely used to enhance photocatalytic reaction rates due to localized surface plasmon resonance (Fig. 9b). The "hot electrons" excited from surface plasmon resonance will be injected into the conduction band of the metal–semiconductor, thus enhancing photocatalytic activity.

Hydrothermal and impregnation methods have been used to develop Ag SACs supported on hollandite manganese dioxides (Ag-HMO) for pCO_2RR to CH_4.[200] During the calcination process, the Ag atoms enter the HMO lattice tunnel through the anti-Oswald maturation mechanism to promote the formation of single-atom Ag chains, while effectively inhibiting Ag agglomeration to improve the catalytic efficiency. Recently, the heterostructured photocatalysts have been considered as an effective strategy to promote the spatial separation of photo-generated electrons and holes. The catalyst with NiMOF/CN heterojunction structure exhibited a photocatalytic activity 18 times larger than pure carbon–nitrogen.[152] The Pd–Au hetero junction model co-catalyst have also been prepared,[175] in which electron-deficient Pd massively inhibited the competition for H_2 generation and enhanced the electron–hole separation, while the electron-rich Au promote the 8-electron reduction of CO_2 to CH_4 at the Pd–Au interface.

Even though the synthetic strategies are continuously innovative, CO and H_2 are still formed along with the pCO_2RR to CH_4, which reduces the selectivity of CH_4. The key for improving the pCO_2RR activity and CH_4 selectivity is preventing or reducing this phenomenon. Otherwise, this aspect of research would play a great potential in the field of theoretical studies of synthetic photocatalysts for pCO_2RR, making it a viable technology for a carbon-neutral future.

3.3 pCO_2RR to CH_3OH

The two main reaction systems for pCO_2RR by water reducing agent are liquid- and gas-phase systems.[205,206] CH_3OH as the reduced liquid product generally exists in liquid phase system. In addition, photocatalytic reduction of H_2O produces relatively strong hydrogen side reactions, which can reduce the selectivity of the products. Therefore, the effects of different catalytic

systems on the reaction products should be taken into account. Kavil *et al.* synthesized Cu/C–TiO_2 nanocatalysts for pCO_2RR to CH_3OH in seawater using sol–gel method by co-doping Cu and C into TiO_2.[207] The pathway followed with thermodynamic principle is:

$$n\mathrm{TiO_2} + 6h\nu \rightarrow 6e_{cb}^{-} + 6h_{vb}^{+} \quad \text{(R-1)}$$

$$6H^{+} + 6e_{cb}^{-} \rightarrow 6H^{\cdot} \quad \text{(R-2)}$$

$$CO_2 + 6H^{\cdot} \rightarrow CH_3OH + H_2O \quad \text{(R-3)}$$

$$6OH^{-} + 6h_{vb}^{+} \rightarrow 3/2\ O_2 + 3H_2O \quad \text{(R-4)}$$

The overall reaction is the following:

$$2CO_2 + 4H_2O \rightarrow 2CH_3OH + 3O_2 \quad \text{(R-5)}$$

It is shown that Cu doping into TiO_2 can effectively trap carriers and inhibit electron–hole recombination, thus effectively improve the efficiency and selectivity for CH_3OH generation. The effects of factors on the pCO_2RR by Cu/C–TiO_2 were investigated. Pan *et al.* used CeO_2/CuO p–n junction photocatalyst with Cu cocatalysts for pCO_2RR to CH_3OH (Fig. 9d).[201] Under light irradiation, the photoexcited electrons in CuO transfer to cerium oxide because the CB of cerium oxide is more positive than that of copper oxide, while the holes (h^+) generated in the VB of CeO_2 under light irradiation will migrate to the VB of CuO. By electron–hole exchange between CuO and CeO_2, electron–hole pair complexation is suppressed and the effectiveness of electron reduction of CO_2 on cerium dioxide nanoparticles is increased. The combination of p-type copper oxide and n-type cerium oxide make the carrier in the cerium oxide nanoparticles/CuO nanoparticles catalyst concentration is 108 times higher than that of the copper oxide nanoparticle catalyst, which greatly improves pCO_2RR performance. Meanwhile simple catalyst modification (*i.e.* cerium dioxide electrodeposition) can significantly increase the carriers' concentration and electron availability, thus chemically reducing CO_2 plasma to valuable commercial chemicals and providing a theoretical model for pCO_2RR.

Cu-based catalysts have been widely applied for pCO_2RR to CH_3OH by different design strategies to increase the active sites and improve the catalytic efficiency. Meanwhile, MOFs are considered as potential light-driven catalysts, which have imidazolium or aromatic carboxylate-based linkers.[208,209] Goyal *et al.* developed a catalyst (CuZrlm) with Cu combined with zirconium oxide loaded on imidazoline skeletons,[13] which can effectively improve the photocatalytic performance of imidazolines as potential catalysts for pCO_2RR to CH_3OH. The authors stated that the presence of Cu^{2+} oxidation state and uniform dispersion of the active metal are the main reasons for the improved yield, because Zr introduction can distort the symmetry of the Cu^{2+} oxidation state thereby stimulating charge transfer.

Although pCO_2RR research has made significant breakthroughs in artificial action and photosynthesis, the industrialization is still limited by high costs, carrier limitations, and imperfect analytical characterization techniques. To further improve the performance of pCO_2RR, we should work on finding new carrier materials and designing different photocatalyst structures, as well as proposing new pathways for pCO_2RR to design highly selective and stable photocatalysts.

4. Conclusions and outlook

In this review, we focus on the theoretical studies of electro- and photo-chemical CO_2RR aspects with SACs. The conversion of CO_2 to CO, CH_4, alcohols, acids and other organics have been discussed in detail. The construction of SACs on different unique support, along with the detail catalytic mechanism and improvement of product selectivity were involved.

In spite of gratifying results on the CO_2RR, the challenges of how to improve the activity and selectivity of CO_2RR products, as well as to find green mild conversion environment for large-scale industrial implementation are still the issues need to be solved in the future. The influences of electrode morphology, surface structure and reaction conditions on CO_2RR are still required to be studied to improve the stability of catalysts. For the theoretical calculations, a multi-scale computational model covering all aspects, rather than a collection of theoretical models applicable to specific cases is also needed to achieve.

Author contributions

Q. Yu supervised the project and organized the collaboration. L. Jiang, Q Yang co-wrote the manuscript with input from all authors. Z. Xia and X. Yu summarized the electro-CO_2RR, M. Zhao and Q. Shi summarized the photo-CO_2RR.

Conflicts of interest

The authors declare that they have no known competing financial interests or personal relationships that could have appeared to influence the work reported in this paper.

Acknowledgements

This work was financially supported by the National Natural Science Foundation of China (No. 92061109), Natural Science Basic Research Program of Shaanxi (No. 2021JCW-20 and 2022KJXX-18), Open Project Program of Fujian Key Laboratory of Functional Marine Sensing Materials (Grant no. MJUKF-FMSM202002). The support by the Guangdong Provincial Key Laboratory of Catalysis (No. 2020B121201002) is also acknowledged.

References

1 Z. Zhang, J. Xiao, X. J. Chen, S. Yu, L. Yu, R. Si, Y. Wang, S. Wang, X. Meng, Y. Wang, Z. Q. Tian and D. Deng, *Angew Chem. Int. Ed.*, 2018, **57**, 16339–16342.
2 Y. Li, H. Su, S. H. Chan and Q. Sun, *ACS Catal.*, 2015, **5**, 6658–6664.

3 B. An, Z. Li, Y. Song, J. Zhang, L. Zeng, C. Wang and W. Lin, *Nat. Catal.*, 2019, **2**, 709–717.
4 Q. Liu, X. Yang, L. Li, S. Miao, Y. Li, Y. Li, X. Wang, Y. Huang and T. Zhang, *Nat. Commun.*, 2017, **8**, 1407.
5 H. Liang, B. Zhang, P. Gao, X. Yu, X. Liu, X. Yang, H. Wu, L. Zhai, S. Zhao, G. Wang, A. Bavel and Y. Qin, *Chem. Catal.*, 2022, **2**, 610–621.
6 Q. He, D. Liu, J. H. Lee, Y. Liu, Z. Xie, S. Hwang, S. Kattel, L. Song and J. G. Chen, *Angew Chem. Int. Ed.*, 2020, **59**, 3033–3037.
7 W. Ni, Z. Liu, Y. Zhang, C. Ma, H. Deng, S. Zhang and S. Wang, *Adv. Mater.*, 2021, **33**, 2003238.
8 M. Zhang, Z. Hu, L. Gu, Q. Zhang, L. Zhang, Q. Song, W. Zhou and S. Hu, *Nano Res.*, 2020, **13**, 3206–3211.
9 Z. Zhao and G. Lu, *J. Phys. Chem. C*, 2019, **123**, 4380–4387.
10 S. Kanan, M. A. Moyet, R. B. Arthur and H. H. Patterson, *Catal. Rev.*, 2019, **62**, 1–65.
11 T. Inoue, A. Fujishima, S. Konishi and K. Honda, *Nature*, 1979, **277**, 637–638.
12 S. N. Habisreutinger, L. Schmidt-Mende and J. K. Stolarczyk, *Angew Chem. Int. Ed.*, 2013, **52**, 7372–7408.
13 S. Goyal, M. S. Shaharun, G. S. Jayabal, C. F. Kait, B. Abdullah and L. J. Wei, *Catalysts*, 2021, **11**, 346.
14 E. A. Dolgopolova, A. M. Rice, C. R. Martin and N. B. Shustova, *Chem. Soc. Rev.*, 2018, **47**, 4710–4728.
15 S. Saini, P. K. Prajapati and S. L. Jain, *Catal. Rev.*, 2020, **64**, 631–677.
16 B. Qiao, A. Wang, X. Yang, L. F. Allard, Z. Jiang, Y. Cui, J. Liu, J. Li and T. Zhang, *Nat. Chem.*, 2011, **3**, 634–641.
17 X. F. Yang, A. Wang, B. Qiao, J. Li, J. Liu and T. Zhang, *Acc. Chem. Res.*, 2013, **46**, 1740–1748.
18 A. Wang, J. Li and T. Zhang, *Nat. Rev. Chem.*, 2018, **2**, 65–81.
19 H. Y. Zhuo, X. Zhang, J. X. Liang, Q. Yu, H. Xiao and J. Li, *Chem. Rev.*, 2020, **120**, 12315–12341.
20 P. Rong, Y.-F. Jiang, Q. Wang, M. Gu, X.-L. Jiang and Q. Yu, *J. Mater. Chem. A*, 2022, **10**, 6231–6241.
21 J.-H. Liu, L.-M. Yang and E. Ganz, *J. Mater. Chem. A*, 2019, **7**, 11944–11952.
22 Y. Wang, M. Wang, Z. Lu, D. Ma and Y. Jia, *Nanoscale*, 2021, **13**, 13390–13400.
23 P. Lv, D. Wu, B. He, X. Li, R. Zhu, G. Tang, Z. Lu, D. Ma and Y. Jia, *J. Mater. Chem. A*, 2022, **10**, 9707–9716.
24 Y. Wang, D. Wu, P. Lv, B. He, X. Li, D. Ma and Y. Jia, *Nanoscale*, 2022, **14**, 10862–10872.
25 D. Wu, B. He, Y. Wang, P. Lv, D. Ma and Y. Jia, *J. Phys. D: Appl. Phys.*, 2022, **55**, 203001.
26 B. He, P. Lv, D. Wu, X. Li, R. Zhu, K. Chu, D. Ma and Y. Jia, *J. Mater. Chem. A*, 2022, **10**, 18690–18700.
27 D. Wu, P. Lv, J. Wu, B. He, X. Li, K. Chu, Y. Jia and D. Ma, *J. Mater. Chem. A*, 2023, **11**, 1817–1828.
28 X. Cui, W. Li, P. Ryabchuk, K. Junge and M. Beller, *Nat. Catal.*, 2018, **1**, 385–397.
29 J. Gu, C. S. Hsu, L. Bai, H. M. Chen and X. Hu, *Science*, 2019, **364**, 1091–1094.
30 B. Zhang, J. Zhang, J. Shi, D. Tan, L. Liu, F. Zhang, C. Lu, Z. Su, X. Tan, X. Cheng, B. Han, L. Zheng and J. Zhang, *Nat. Commun.*, 2019, **10**, 2980.
31 T. N. Nguyen, M. Salehi, Q. V. Le, A. Seifitokaldani and C. T. Dinh, *ACS Catal.*, 2020, **10**, 10068–10095.
32 J. J. Masana, J. Xiao, H. Zhang, X. Lu, M. Qiu and Y. Yu, *Appl. Catal. B Environ.*, 2023, **323**, 122199.
33 G. Hai and H. Wang, *Coord. Chem. Rev.*, 2022, **469**, 214670.
34 K. R. Phillips, Y. Katayama, J. Hwang and Y. Shao-Horn, *J. Phys. Chem. Lett.*, 2018, **9**, 4407–4412.
35 S. Chen, Y. Li, Z. Bu, F. Yang, J. Luo, Q. An, Z. Zeng, J. Wang and S. Deng, *J. Mater. Chem. A*, 2021, **9**, 1705–1712.
36 D. Xue, H. Xia, W. Yan, J. Zhang and S. Mu, *Nanomicro Lett.*, 2020, **13**, 5.
37 Q. H. Low, N. W. X. Loo, F. Calle-Vallejo and B. S. Yeo, *Angew Chem. Int. Ed.*, 2019, **58**, 2256–2260.
38 A. Guan, Z. Chen, Y. Quan, C. Peng, Z. Wang, T.-K. Sham, C. Yang, Y. Ji, L. Qian, X. Xu and G. Zheng, *ACS Energy Lett.*, 2020, **5**, 1044–1053.
39 Y. Liu, H. Zhu, Z. Zhao, N. Huang, P. Liao and X. Chen, *ACS Catal.*, 2022, **12**, 2749–2755.
40 Y. Sun, Z. Xue, Q. Liu, Y. Jia, Y. Li, K. Liu, Y. Lin, M. Liu, G. Li and C. Y. Su, *Nat. Commun.*, 2021, **12**, 1369.
41 J. D. Benck, T. R. Hellstern, J. Kibsgaard, P. Chakthranont and T. F. Jaramillo, *ACS Catal.*, 2014, **4**, 3957–3971.
42 C. Gao, S. Chen, Y. Wang, J. Wang, X. Zheng, J. Zhu, L. Song, W. Zhang and Y. Xiong, *Adv. Mater.*, 2018, **30**, 1704624.
43 T. Zheng, K. Jiang and H. Wang, *Adv. Mater.*, 2018, **30**, 1802066.
44 R. Kortlever, J. Shen, K. J. Schouten, F. Calle-Vallejo and M. T. Koper, *J. Phys. Chem. Lett.*, 2015, **6**, 4073–4082.
45 H. Zhang, J. Li, S. Xi, Y. Du, X. Hai, J. Wang, H. Xu, G. Wu, J. Zhang, J. Lu and J. Wang, *Angew Chem. Int. Ed.*, 2019, **58**, 14871–14876.
46 Y. Pan, R. Lin, Y. Chen, S. Liu, W. Zhu, X. Cao, W. Chen, K. Wu, W. C. Cheong, Y. Wang, L. Zheng, J. Luo, Y. Lin, Y. Liu, C. Liu, J. Li, Q. Lu, X. Chen, D. Wang, Q. Peng, C. Chen and Y. Li, *J. Am. Chem. Soc.*, 2018, **140**, 4218–4221.
47 Y. Zhang, L. Jiao, W. Yang, C. Xie and H. L. Jiang, *Angew Chem. Int. Ed.*, 2021, **60**, 7607–7611.
48 Q. He, J. H. Lee, D. Liu, Y. Liu, Z. Lin, Z. Xie, S. Hwang, S. Kattel, L. Song and J. G. Chen, *Adv. Funct. Mater.*, 2020, **30**, 2000407.
49 C. Xu, X. Zhi, A. Vasileff, D. Wang, B. Jin, Y. Jiao, Y. Zheng and S.-Z. Qiao, *Small Structures*, 2020, **2**, 2000058.
50 M. Fang, X. Wang, X. Li, Y. Zhu, G. Xiao, J. Feng, X. Jiang, K. Lv, Y. Zhu and W. F. Lin, *ChemCatChem*, 2020, **13**, 603–609.
51 Y. Hou, Y.-L. Liang, P.-C. Shi, Y.-B. Huang and R. Cao, *Appl. Catal. B Environ.*, 2020, **271**, 118929.
52 H. Cheng, X. Wu, X. Li, X. Nie, S. Fan, M. Feng, Z. Fan, M. Tan, Y. Chen and G. He, *Chem. Eng. J.*, 2021, **407**, 126842.
53 H.-L. Zhu, Y.-Q. Zheng and M. Shui, *ACS Appl. Energy Mater.*, 2020, **3**, 3893–3901.
54 C. He, Y. Zhang, Y. Zhang, L. Zhao, L. P. Yuan, J. Zhang, J. Ma and J. S. Hu, *Angew Chem. Int. Ed.*, 2020, **59**, 4914–4919.
55 J. Tuo, Y. Zhu, H. Jiang, J. Shen and C. Li, *ChemElectroChem*, 2020, **7**, 4767–4772.

56 F. Pan, B. Li, E. Sarnello, Y. Fei, X. Feng, Y. Gang, X. Xiang, L. Fang, T. Li, Y. H. Hu, G. Wang and Y. Li, *ACS Catal.*, 2020, **10**, 10803–10811.
57 Q. Cheng, K. Mao, L. Ma, L. Yang, L. Zou, Z. Zou, Z. Hu and H. Yang, *ACS Energy Lett.*, 2018, **3**, 1205–1211.
58 W. Ni, Y. Xue, X. Zang, C. Li, H. Wang, Z. Yang and Y. M. Yan, *ACS Nano*, 2020, **14**, 2014–2023.
59 X. Yang, J. Cheng, X. Xuan, N. Liu and J. Liu, *ACS Sustainable Chem. Eng.*, 2020, **8**, 10536–10543.
60 W. Ren, X. Tan, W. Yang, C. Jia, S. Xu, K. Wang, S. C. Smith and C. Zhao, *Angew Chem. Int. Ed.*, 2019, **58**, 6972–6976.
61 K. Jiang, S. Siahrostami, T. Zheng, Y. Hu, S. Hwang, E. Stavitski, Y. Peng, J. Dynes, M. Gangisetty, D. Su, K. Attenkofer and H. Wang, *Energy Environ. Sci.*, 2018, **11**, 893–903.
62 T. Möller, W. Ju, A. Bagger, X. Wang, F. Luo, T. Ngo Thanh, A. S. Varela, J. Rossmeisl and P. Strasser, *Energy Environ. Sci.*, 2019, **12**, 640–647.
63 H.-Y. Jeong, M. Balamurugan, V. S. K. Choutipalli, E.-s. Jeong, V. Subramanian, U. Sim and K. T. Nam, *J. Mater. Chem. A*, 2019, **7**, 10651–10661.
64 R. Daiyan, X. Lu, X. Tan, X. Zhu, R. Chen, S. C. Smith and R. Amal, *ACS Appl. Energy Mater.*, 2019, **2**, 8002–8009.
65 H. Wang, M. Li, G. Liu, L. Yang, P. Sun and S. Sun, *New J. Chem.*, 2021, **45**, 1063–1071.
66 X. Zhang, Y. Wang, M. Gu, M. Wang, Z. Zhang, W. Pan, Z. Jiang, H. Zheng, M. Lucero, H. Wang, G. E. Sterbinsky, Q. Ma, Y.-G. Wang, Z. Feng, J. Li, H. Dai and Y. Liang, *Nat. Energy*, 2020, **5**, 684–692.
67 C. Xu, A. Vasileff, Y. Zheng and S. Z. Qiao, *Adv. Mater. Interfac.*, 2020, **8**, 2001904.
68 Q. Fan, P. Hou, C. Choi, T. S. Wu, S. Hong, F. Li, Y. L. Soo, P. Kang, Y. Jung and Z. Sun, *Adv. Energy Mater.*, 2019, **10**, 1903068.
69 C. Chen, X. Sun, X. Yan, Y. Wu, H. Liu, Q. Zhu, B. B. A. Bediako and B. Han, *Angew Chem. Int. Ed.*, 2020, **59**, 11123–11129.
70 L. Lu, W. Guo, C. Chen, Q. Zhu, J. Ma, H. Wu, D. Yang, G. Yang, X. Sun and B. Han, *Green Chem.*, 2020, **22**, 6804–6808.
71 W. Guo, J. Bi, Q. Zhu, J. Ma, G. Yang, H. Wu, X. Sun and B. Han, *ACS Sustainable Chem. Eng.*, 2020, **8**, 12561–12567.
72 X. Sun, C. Chen, S. Liu, S. Hong, Q. Zhu, Q. Qian, B. Han, J. Zhang and L. Zheng, *Angew Chem. Int. Ed.*, 2019, **58**, 4669–4673.
73 Q. Cui, G. Qin, W. Wang, L. Sun, A. Du and Q. Sun, *Beilstein J. Nanotechnol.*, 2019, **10**, 540–548.
74 Y. Feng, W. An, Z. Wang, Y. Wang, Y. Men and Y. Du, *ACS Sustainable Chem. Eng.*, 2019, **8**, 210–222.
75 O. Mohan, R. Xu and S. H. Mushrif, *J. Phys. Chem. C*, 2021, **125**, 4041–4055.
76 Y. Wang, H. Arandiyan, J. Scott, K.-F. Aguey-Zinsou and R. Amal, *ACS Appl. Energy Mater.*, 2018, **1**, 6781–6789.
77 H. Guzmán, N. Russo and S. Hernández, *Green Chem.*, 2021, **23**, 1896–1920.
78 C. S. Lo, R. Radhakrishnan and B. L. Trout, *Catal. Today*, 2005, **105**, 93–105.
79 M. M. Shi, D. Bao, B. R. Wulan, Y. H. Li, Y. F. Zhang, J. M. Yan and Q. Jiang, *Adv. Mater.*, 2017, **29**, 1606550.
80 C. T. Dinh, T. Burdyny, M. G. Kibria, A. Seifitokaldani, C. M. Gabardo, F. P. Garcia de Arquer, A. Kiani, J. P. Edwards, P. De Luna, O. S. Bushuyev, C. Zou, R. Quintero-Bermudez, Y. Pang, D. Sinton and E. H. Sargent, *Science*, 2018, **360**, 783–787.
81 H. Tian, H. Tian, S. Wang, S. Chen, F. Zhang, L. Song, H. Liu, J. Liu and G. Wang, *Nat. Commun.*, 2020, **11**, 5025.
82 X. Fang, Q. Shang, Y. Wang, L. Jiao, T. Yao, Y. Li, Q. Zhang, Y. Luo and H. L. Jiang, *Adv. Mater.*, 2018, **30**, 1705112.
83 H. Yang, L. Shang, Q. Zhang, R. Shi, G. I. N. Waterhouse, L. Gu and T. Zhang, *Nat. Commun.*, 2019, **10**, 4585.
84 J. Li, Q. Guan, H. Wu, W. Liu, Y. Lin, Z. Sun, X. Ye, X. Zheng, H. Pan, J. Zhu, S. Chen, W. Zhang, S. Wei and J. Lu, *J. Am. Chem. Soc.*, 2019, **141**, 14515–14519.
85 Q. Zhao, C. Zhang, R. Hu, Z. Du, J. Gu, Y. Cui, X. Chen, W. Xu, Z. Cheng, S. Li, B. Li, Y. Liu, W. Chen, C. Liu, J. Shang, L. Song and S. Yang, *ACS Nano*, 2021, **15**, 4927–4936.
86 Z. Lu, Y. Cheng, S. Li, Z. Yang and R. Wu, *Appl. Surf. Sci.*, 2020, **528**, 147047.
87 H. Li, L. Wang, Y. Dai, Z. Pu, Z. Lao, Y. Chen, M. Wang, X. Zheng, J. Zhu, W. Zhang, R. Si, C. Ma and J. Zeng, *Nat. Nanotechnol.*, 2018, **13**, 411–417.
88 M. Li, B. Hua, L.-C. Wang, Z. Zhou, K. J. Stowers and D. Ding, *Catal. Today*, 2022, **388–389**, 403–409.
89 Y. Wu, Z. Jiang, X. Lu, Y. Liang and H. Wang, *Nature*, 2019, **575**, 639–642.
90 H. Yang, Y. Wu, G. Li, Q. Lin, Q. Hu, Q. Zhang, J. Liu and C. He, *J. Am. Chem. Soc.*, 2019, **141**, 12717–12723.
91 J. Liu, D. Yang, Y. Zhou, G. Zhang, G. Xing, Y. Liu, Y. Ma, O. Terasaki, S. Yang and L. Chen, *Angew. Chem., Int. Ed.*, 2021, **60**, 14473–14479.
92 T. Sun, S. Mitchell, J. Li, P. Lyu, X. Wu, J. Perez-Ramirez and J. Lu, *Adv. Mater.*, 2021, **33**, 2003075.
93 X. Bai, Q. Li, L. Shi, X. Niu, C. Ling and J. Wang, *Small*, 2020, **16**, 1901981.
94 X. Ye, C. Yang, X. Pan, J. Ma, Y. Zhang, Y. Ren, X. Liu, L. Li and Y. Huang, *J. Am. Chem. Soc.*, 2020, **142**, 19001–19005.
95 T. Kiko, Y. Kashima, D. Kanno, T. Watanabe, Y. Tadano, T. Sugie, K. Kobayashi and T. Fujita, *J. Am. Coll. Cardiol.*, 2016, **67**, S224–S225.
96 R. Sun, Y. Liao, S.-T. Bai, M. Zheng, C. Zhou, T. Zhang and B. F. Sels, *Energy Environ. Sci.*, 2021, **14**, 1247–1285.
97 H. Shang, T. Wang, J. Pei, Z. Jiang, D. Zhou, Y. Wang, H. Li, J. Dong, Z. Zhuang, W. Chen, D. Wang, J. Zhang and Y. Li, *Angew Chem. Int. Ed.*, 2020, **59**, 22465–22469.
98 G. Hai, X. Xue, S. Feng, Y. Ma and X. Huang, *ACS Catal.*, 2022, **12**, 15271–15281.
99 Y. Meng, K. Li, D. Xiao, Y. Yuan, Y. Wang and Z. Wu, *Int. J. Hydrogen Energy*, 2020, **45**, 14311–14319.
100 Z. Feng, G. Su, H. Ding, Y. Ma, Y. Li, Y. Tang and X. Dai, *Mol. Catal.*, 2020, **494**, 111142.
101 K. Mori, T. Taga and H. Yamashita, *ACS Catal.*, 2017, **7**, 3147–3151.

102 Z. Chen, T. Fan, Y.-Q. Zhang, J. Xiao, M. Gao, N. Duan, J. Zhang, J. Li, Q. Liu, X. Yi and J.-L. Luo, *Appl. Catal. B Environ.*, 2020, **261**, 118243.
103 X. Shao, X. Yang, J. Xu, S. Liu, S. Miao, X. Liu, X. Su, H. Duan, Y. Huang and T. Zhang, *Chem*, 2019, **5**, 693–705.
104 Q. Wang, S. Santos, C. A. Urbina-Blanco, W. Y. Hernández, M. Impéror-Clerc, E. I. Vovk, M. Marinova, O. Ersen, W. Baaziz, O. V. Safonova, A. Y. Khodakov, M. Saeys and V. V. Ordomsky, *Appl. Catal. B Environ.*, 2021, **290**, 120036.
105 H. Ning, Q. Mao, W. Wang, Z. Yang, X. Wang, Q. Zhao, Y. Song and M. Wu, *J. Alloys Compd.*, 2019, **785**, 7–12.
106 J. Yuan, M.-P. Yang, Q.-L. Hu, S.-M. Li, H. Wang and J.-X. Lu, *J. CO2 Util.*, 2018, **24**, 334–340.
107 A. Javier, B. Chmielowiec, J. Sanabria-Chinchilla, Y.-G. Kim, J. H. Baricuatro and M. P. Soriaga, *Electrocatalysis*, 2015, **6**, 127–131.
108 K. U. D. Calvinho, A. B. Laursen, K. M. K. Yap, T. A. Goetjen, S. Hwang, N. Murali, B. Mejia-Sosa, A. Lubarski, K. M. Teeluck, E. S. Hall, E. Garfunkel, M. Greenblatt and G. C. Dismukes, *Energy Environ. Sci.*, 2018, **11**, 2550–2559.
109 X. Wei, Z. Yin, K. Lyu, Z. Li, J. Gong, G. Wang, L. Xiao, J. Lu and L. Zhuang, *ACS Catal.*, 2020, **10**, 4103–4111.
110 Z. Wang, J. Zhao and Q. Cai, *Phys. Chem. Chem. Phys.*, 2017, **19**, 23113–23121.
111 C. Wang, C. Zhu, M. Zhang, Y. Geng and Z. Su, *Adv. Theory Simul.*, 2020, **3**, 2000218.
112 X. F. Qiu, H. L. Zhu, J. R. Huang, P. Q. Liao and X. M. Chen, *J. Am. Chem. Soc.*, 2021, **143**, 7242–7246.
113 S. Fu, X. Liu, J. Ran, Y. Jiao and S.-Z. Qiao, *Appl. Surf. Sci.*, 2021, **540**, 148293.
114 Y. Jiao, Y. Zheng, P. Chen, M. Jaroniec and S. Z. Qiao, *J. Am. Chem. Soc.*, 2017, **139**, 18093–18100.
115 C. F. Wen, M. Zhou, P. F. Liu, Y. Liu, X. Wu, F. Mao, S. Dai, B. Xu, X. L. Wang, Z. Jiang, P. Hu, S. Yang, H. F. Wang and H. G. Yang, *Angew. Chem., Int. Ed.*, 2022, **61**, e202111700.
116 D. Gao, T. Liu, G. Wang and X. Bao, *ACS Energy Lett.*, 2021, **6**, 713–727.
117 J. Xi, H. S. Jung, Y. Xu, F. Xiao, J. W. Bae and S. Wang, *Adv. Funct. Mater.*, 2021, **31**, 2008318.
118 B. Peng, H. Liu, Z. Liu, X. Duan and Y. Huang, *J. Phys. Chem. Lett.*, 2021, **12**, 2837–2847.
119 A. Kudo and Y. Miseki, *Chem. Soc. Rev.*, 2009, **38**, 253–278.
120 L. Matějová, K. Kočí, M. Reli, L. Čapek, V. Matějka, O. Šolcová and L. Obalová, *Appl. Surf. Sci.*, 2013, **285**, 688–696.
121 H. Zhang, T. Itoi, T. Konishi and Y. Izumi, *J. Am. Chem. Soc.*, 2019, **141**, 6292–6301.
122 J. Yang, J. Hao, S. Xu, Q. Wang, J. Dai, A. Zhang and X. Pang, *ACS Appl. Mater. Interfaces*, 2019, **11**, 32025–32037.
123 S. Yan, J. Wang, H. Gao, N. Wang, H. Yu, Z. Li, Y. Zhou and Z. Zou, *Adv. Funct. Mater.*, 2013, **23**, 1839–1845.
124 X. Chen, S. Shen, L. Guo and S. S. Mao, *Chem. Rev.*, 2010, **110**, 6503–6570.
125 K. Teramura, S.-i. Okuoka, H. Tsuneoka, T. Shishido and T. Tanaka, *Appl. Catal. B Environ.*, 2010, **96**, 565–568.
126 X. F. Xie, X. Y. Dao, F. Guo, X. Y. Zhang, F. M. Wang and W. Y. Sun, *ChemistrySelect*, 2020, **5**, 4001–4007.
127 K. Kočí, P. Praus, M. Edelmannová, N. Ambrožová, I. Troppová, D. Fridrichová, G. Słowik and J. Ryczkowski, *J. Nanosci. Nanotechnol.*, 2017, **17**, 4041–4047.
128 D. V. Markovskaya, S. V. Cherepanova, E. Y. Gerasimov, A. V. Zhurenok, A. V. Selivanova, D. S. Selishchev and E. A. Kozlova, *RSC Adv.*, 2020, **10**, 1341–1350.
129 M. Zhou, S. Wang, P. Yang, C. Huang and X. Wang, *ACS Catal.*, 2018, **8**, 4928–4936.
130 B. Zhou, X. Kong, S. Vanka, S. Cheng, N. Pant, S. Chu, P. Ghamari, Y. Wang, G. Botton, H. Cuo and Z. Mi, *Energy Environ. Sci.*, 2019, **12**, 2842–2848.
131 N. T. P. Le Chi, N. T. Dieu Cam, D. Van Thuan, T. T. Truong, N. T. Thanh Truc, C. Van Hoang, T. T. Thu Phuong, T.-D. Pham, M. H. Thanh Tung, N. T. Minh Thu, N. M. Phuong and V. N. Nguyen, *Appl. Surf. Sci.*, 2019, **467–468**, 1249–1255.
132 N. Dewangan, W. M. Hui, S. Jayaprakash, A.-R. Bawah, A. J. Poerjoto, T. Jie, A. Jangam, K. Hidajat and S. Kawi, *Catal. Today*, 2020, **356**, 490–513.
133 S. Goyal, M. Shaharun, C. Kait, B. Abdullah and M. Ameen, *Catalysts*, 2018, **8**, 581.
134 G. Gao, Y. Jiao, E. R. Waclawik and A. Du, *J. Am. Chem. Soc.*, 2016, **138**, 6292–6297.
135 D. Mateo, A. M. Asiri, J. Albero and H. Garcia, *Photochem. Photobiol. Sci.*, 2018, **17**, 829–834.
136 H. Wei, X. Liu, A. Wang, L. Zhang, B. Qiao, X. Yang, Y. Huang, S. Miao, J. Liu and T. Zhang, *Nat. Commun.*, 2014, **5**, 5634.
137 T. Yang, R. Fukuda, S. Hosokawa, T. Tanaka, S. Sakaki and M. Ehara, *ChemCatChem*, 2017, **9**, 1222–1229.
138 Z. Luo, Z. Wang, J. Li, K. Yang and G. Zhou, *Phys. Chem. Chem. Phys.*, 2020, **22**, 11392–11399.
139 J. Li, H. Huang, P. Liu, X. Song, D. Mei, Y. Tang, X. Wang and C. Zhong, *J. Catal.*, 2019, **375**, 351–360.
140 Y. N. Gong, L. Jiao, Y. Qian, C. Y. Pan, L. Zheng, X. Cai, B. Liu, S. H. Yu and H. L. Jiang, *Angew Chem. Int. Ed.*, 2020, **59**, 2705–2709.
141 M. R. Axet, J. Durand, M. Gouygou and P. Serp, *Adv. Organomet. Chem.*, 2019, **71**, 53–174.
142 H. Zhang, W. Tian, X. Duan, H. Sun, Y. Shen, G. Shao and S. Wang, *Nanoscale*, 2020, **12**, 6937–6952.
143 J. Jiang, F. Sun, S. Zhou, W. Hu, H. Zhang, J. Dong, Z. Jiang, J. Zhao, J. Li, W. Yan and M. Wang, *Nat. Commun.*, 2018, **9**, 2885.
144 Y. Chen, H. Hong, J. Cai and Z. Li, *ChemCatChem*, 2020, **13**, 656–663.
145 M. Tahir and N. S. Amin, *Appl. Catal., A*, 2015, **493**, 90–102.
146 X. Wang, Z. Zhang, Z. Huang, P. Dong, X. Nie, Z. Jin and X. Zhang, *Mater. Res. Bull.*, 2019, **118**, 110502.
147 H. She, Z. Zhao, W. Bai, J. Huang, L. Wang and Q. Wang, *Mater. Res. Bull.*, 2020, **124**, 110758.
148 Y. Ma, B. Chi, W. Liu, L. Cao, Y. Lin, X. Zhang, X. Ye, S. Wei and J. Lu, *ACS Catal.*, 2019, **9**, 8404–8412.
149 Z. Jiang, M. Jing, X. Feng, J. Xiong, C. He, M. Douthwaite, L. Zheng, W. Song, J. Liu and Z. Qu, *Appl. Catal. B Environ.*, 2020, **278**, 119304.

150 D. Sun, Y. Gao, J. Fu, X. Zeng, Z. Chen and Z. Li, *Chem. Commun.*, 2015, **51**, 2645–2648.
151 C. Zheng, X. Qiu, J. Han, Y. Wu and S. Liu, *ACS Appl. Mater. Interfaces*, 2019, **11**, 42243–42249.
152 L. Zhao, Z. Zhao, Y. Li, X. Chu, Z. Li, Y. Qu, L. Bai and L. Jing, *Nanoscale*, 2020, **12**, 10010–10018.
153 J. Low, J. Yu and W. Ho, *J. Phys. Chem. Lett.*, 2015, **6**, 4244–4251.
154 R. Zhou, Y. Yin, D. Long, J. Cui, H. Yan, W. Liu and J. H. Pan, *Prog. Nat. Sci.*, 2019, **29**, 660–666.
155 X.-Y. Dao, X.-F. Xie, J.-H. Guo, X.-Y. Zhang, Y.-S. Kang and W.-Y. Sun, *ACS Appl. Energy Mater.*, 2020, **3**, 3946–3954.
156 X. Hu, J. Hu, Q. Peng, X. Ma, S. Dong and H. Wang, *Mater. Res. Bull.*, 2020, **122**, 110682.
157 Z. Zhu, Z. Liu, X. Tang, K. Reeti, P. Huo, J. W.-C. Wong and J. Zhao, *Catal. Sci. Technol.*, 2021, **11**, 1725–1736.
158 L. Tan, K. Peter, J. Ren, B. Du, X. Hao, Y. Zhao and Y.-F. Song, *Front. Chem. Sci. Eng.*, 2020, **15**, 99–108.
159 S. Das and K. parida, *Mater. Today Proc.*, 2021, **35**, 275–280.
160 X. Liu, S. Inagaki and J. Gong, *Angew Chem. Int. Ed.*, 2016, **55**, 14924–14950.
161 Z. Guo, S. Cheng, C. Cometto, E. Anxolabehere-Mallart, S. M. Ng, C. C. Ko, G. Liu, L. Chen, M. Robert and T. C. Lau, *J. Am. Chem. Soc.*, 2016, **138**, 9413–9416.
162 C. Yang and Z.-Y. Zhao, *Comput. Mater. Sci.*, 2018, **151**, 160–173.
163 Y. Wang, Y. Chen, Q. Hou, M. Ju and W. Li, *Nanomaterials*, 2019, **9**, 391.
164 J. Di, C. Chen, S. Z. Yang, S. Chen, M. Duan, J. Xiong, C. Zhu, R. Long, W. Hao, Z. Chi, H. Chen, Y. X. Weng, J. Xia, L. Song, S. Li, H. Li and Z. Liu, *Nat. Commun.*, 2019, **10**, 2840.
165 J. Wang, T. Heil, B. Zhu, C.-W. Tung, J. Yu, H. M. Chen, M. Antonietti and S. Cao, *ACS Nano*, 2020, **14**, 8584–8593.
166 O. K. Varghese, M. Paulose, T. J. Latempa and C. A. Grimes, *Nano Lett.*, 2009, **9**, 731–737.
167 W. Tu, Y. Zhou and Z. Zou, *Adv. Mater.*, 2014, **26**, 4607–4626.
168 S. Zhu, S. Liang, Y. Tong, X. An, J. Long, X. Fu and X. Wang, *Phys. Chem. Chem. Phys.*, 2015, **17**, 9761–9770.
169 Y. Liu, S. Zhou, J. Li, Y. Wang, G. Jiang, Z. Zhao, B. Liu, X. Gong, A. Duan, J. Liu, Y. Wei and L. Zhang, *Appl. Catal. B Environ.*, 2015, **168–169**, 125–131.
170 N. Li, Y. Li, R. Jiang, J. Zhou and M. Liu, *Appl. Surf. Sci.*, 2019, **498**, 143861.
171 X. Li, J. Wen, J. Low, Y. Fang and J. Yu, *Sci. China Mater.*, 2014, **57**, 70–100.
172 M. Tahir and B. Tahir, *Appl. Surf. Sci.*, 2016, **377**, 244–252.
173 Y. Yang, F. Li, J. Chen, J. Fan and Q. Xiang, *ChemSusChem*, 2020, **13**, 1979–1985.
174 Y. Ji and Y. Luo, *ACS Catal.*, 2016, **6**, 2018–2025.
175 X. Cai, J. Wang, R. Wang, A. Wang, S. Zhong, J. Chen and S. Bai, *J. Mater. Chem. A*, 2019, **7**, 5266–5276.
176 A. H. Chowdhury, A. Das, S. Riyajuddin, K. Ghosh and S. M. Islam, *Catal. Sci. Technol.*, 2019, **9**, 6566–6569.
177 T. Li, C. Wang, T. Wang and L. Zhu, *Appl. Catal. B Environ.*, 2020, **268**, 118442.
178 J. He, P. Lv, J. Zhu and H. Li, *RSC Adv.*, 2020, **10**, 22460–22467.
179 H. Guo, M. Chen, Q. Zhong, Y. Wang, W. Ma and J. Ding, *J. CO2 Util.*, 2019, **33**, 233–241.
180 F. Li, X. Chen, Q. Guo, D. Dai and X. Yang, *J. Phys. Chem. C*, 2020, **124**, 8766–8774.
181 J. Li, B. Huang, Q. Guo, S. Guo, Z. Peng, J. Liu, Q. Tian, Y. Yang, Q. Xu, Z. Liu and B. Liu, *Appl. Catal. B Environ.*, 2021, **284**, 119733.
182 M. Mohamedali, O. Ayodele and H. Ibrahim, *Renew. Sustain. Energy Rev.*, 2020, **131**, 110024.
183 X. Yu, V. V. Ordomsky and A. Y. Khodakov, *ChemCatChem*, 2020, **12**, 740–749.
184 X. Zhang, G. Ren, C. Zhang, R. Li, Q. Zhao and C. Fan, *Catal. Lett.*, 2020, **150**, 2510–2516.
185 Z. Sun, N. Talreja, H. Tao, J. Texter, M. Muhler, J. Strunk and J. Chen, *Angew Chem. Int. Ed.*, 2018, **57**, 7610–7627.
186 F. Almomani, R. Bhosale, M. Khraisheh, A. Kumar and M. Tawalbeh, *Appl. Surf. Sci.*, 2019, **483**, 363–372.
187 S. Nahar, M. F. M. Zain, A. A. H. Kadhum, H. A. Hasan and M. R. Hasan, *Materials*, 2017, **10**, 629.
188 N. Sasirekha, S. Basha and K. Shanthi, *Appl. Catal. B Environ.*, 2006, **62**, 169–180.
189 K. Mori, H. Yamashita and M. Anpo, *RSC Adv.*, 2012, **2**, 3165–3172.
190 I. A. Shkrob, T. W. Marin, H. He and P. Zapol, *J. Phys. Chem. C*, 2012, **116**, 9450–9460.
191 V. P. Indrakanti, H. H. Schobert and J. D. Kubicki, *Energy Fuels*, 2009, **23**, 5247–5256.
192 Y. Li, B. Li, D. Zhang, L. Cheng and Q. Xiang, *ACS Nano*, 2020, **14**, 10552–10561.
193 S. Ji, Y. Qu, T. Wang, Y. Chen, G. Wang, X. Li, J. Dong, Q. Chen, W. Zhang, Z. Zhang, S. Liang, R. Yu, Y. Wang, D. Wang and Y. Li, *Angew Chem. Int. Ed.*, 2020, **59**, 10651–10657.
194 W. Zhong, R. Sa, L. Li, Y. He, L. Li, J. Bi, Z. Zhuang, Y. Yu and Z. Zou, *J. Am. Chem. Soc.*, 2019, **141**, 7615–7621.
195 X. Xiong, C. Mao, Z. Yang, Q. Zhang, G. I. N. Waterhouse, L. Gu and T. Zhang, *Adv. Energy Mater.*, 2020, **10**, 2002928.
196 K. Xie, N. Umezawa, N. Zhang, P. Reunchan, Y. Zhang and J. Ye, *Energy Environ. Sci.*, 2011, **4**, 4211–4219.
197 S. Chen, G. Hai, H. Gao, X. Chen, A. Li and X. Zhang, *Chem. Eng. J.*, 2021, **406**, 126886.
198 Y. Ji and Y. Luo, *J. Am. Chem. Soc.*, 2016, **138**, 15896–15902.
199 C. Boerigter, R. Campana, M. Morabito and S. Linic, *Nat. Commun.*, 2016, **7**, 10545.
200 J. Ding, X. Liu, M. Shi, T. Li, M. Xia, X. Du, R. Shang, H. Gu and Q. Zhong, *Sol. Energy Mater. Sol. Cells*, 2019, **195**, 34–42.
201 Z. Pan, E. Han, J. Zheng, J. Lu, X. Wang, Y. Yin, G. I. N. Waterhouse, X. Wang and P. Li, *Nanomicro Lett.*, 2020, **12**, 18.
202 S. Kawamura, H. Zhang, M. Tamba, T. Kojima, M. Miyano, Y. Yoshida, M. Yoshiba and Y. Izumi, *J. Catal.*, 2017, **345**, 39–52.
203 Q. Liu, Q. Chen, T. Li, Q. Ren, S. Zhong, Y. Zhao and S. Bai, *J. Mater. Chem. A*, 2019, **7**, 27007–27015.

204 S. S. Bhosale, A. K. Kharade, E. Jokar, A. Fathi, S. M. Chang and E. W. Diau, *J. Am. Chem. Soc.*, 2019, **141**, 20434–20442.
205 J. Hong, W. Zhang, Y. Wang, T. Zhou and R. Xu, *ChemCatChem*, 2014, **6**, 2315–2321.
206 T. Ohno, N. Murakami, T. Koyanagi and Y. Yang, *J. CO2 Util.*, 2014, **6**, 17–25.
207 Y. N. Kavil, Y. A. Shaban, R. K. Al Farawati, M. I. Orif, M. Zobidi and S. U. M. Khan, *Water, Air, Soil Pollut.*, 2018, **229**, 236.
208 S.-T. Gao, W.-H. Liu, N.-Z. Shang, C. Feng, Q.-H. Wu, Z. Wang and C. Wang, *RSC Adv.*, 2014, **4**, 61736–61742.
209 Q. Liu, Z.-X. Low, L. Li, A. Razmjou, K. Wang, J. Yao and H. Wang, *J. Mater. Chem. A*, 2013, **1**, 11563–11569.